HIGHER-ORDER MOMENT MODELS FOR MULTIPHASE FLOWS COUPLED TO A BACKGROUND GAS

A Thesis Submitted to

the Faculty of Graduate and Postdoctoral Studies

by

François Forgues

In Partial Fulfillment of the Requirements for the Degree of

MASTERS OF APPLIED SCIENCE

in Mechanical Engineering

Department of Mechanical Engineering

University of Ottawa

Ottawa, Canada

© François Forgues, Ottawa, Canada, 2019

Acknowledgements

To begin, I would like to express my sincere gratitude to my advisor, Professor James McDonald. I was fortunate to have his continuous support during my Master study and related research. His patience, motivation, and immense knowledge guided me during my research and when writing this thesis. His open-door policy provided answers to my many questions. Without hesitation, he was keen to share his passion and knowledge in fluid mechanics and moment closure with me. I cannot imagine having a better advisor and mentor for my Master study.

Along with my advisor, I would like to thank the rest of my thesis committee: Professor Matei Radulescu from University of Ottawa and Professor Edgar A. Matida from Carleton University for their insightful comments and words of encouragement, but mostly for asking the hard questions that provided me with the motivation to broaden my research, looking at various perspectives.

My sincere thanks also goes to Dr.Lucian Ivan from the Canadian Nuclear Laboratories, who also provided me with excellent guidance in my research, in conjunction with the Canadian Laboratory. I am grateful to the Canadian Nuclear Laboratories for their interest in funding my research. Without the support from this organization, it would have not been possible to conduct this research.

I want to thank my fellow students and great friends for the stimulating discussions, for the countless hours spent together in the computer lab, and for all the great memories we made over the last two years.

Last but not the least, I would like to thank my parents, my brother, and sister for their on-going support, for believing in my abilities to write this thesis. And finally, I would be remiss not to thank Lucy for always being the first to greet me at the door and welcome me after a long day at school.

Abstract

Modelling of laminar multiphase flow is extremely important in a wide range of engineering and scientific applications. The particle phases are often difficult to model, especially when particles display a range of sizes and velocities at each location in space. Lagrangian methods can be too expensive and many Eulerian methods, though often computationally more affordable, suffer from model deficiencies and mathematical artifacts that lead to non-physical results. For example, efficient Eulerian models that can accurately predict the crossing of multiple streams of non-interacting particles in laminar flow have traditionally been lacking. The predictive capabilities of modern techniques from the kinetic theory of gases to the treatment of disperse multiphase flows are investigated. In particular, several moment-methods, including a recently proposed fourteen-moment approximation to the underlying kinetic equation describing particle motion, are considered and their abilities to predict particle-stream crossing are assessed. Furthermore, a new polydisperse model has been proposed for treatment of flows that display a range of particles sizes. The proposed model is an extension of the well-known maximum-entropy ten-moment model from rarefied gas dynamics with an addition for the treatment of a range of particle diameters. This model allows for anisotropic variance of particle velocities in phase space and directly treats correlations between particle diameter and velocity. The derivation and mathematical structure, of the proposed models are presented. A fine-volume discretization solution procedure for the resulting moment equations is described and used for performing numerical experiments. Results for flow problems that are designed to demonstrate the fundamental behaviour of each model are presented. It is shown that the new models offer clear advantages in terms of accuracy as compared to traditional Eulerian models for multiphase flows.

Keywords: Multiphase Flow, Kinetic Theory, Moment Method, Polydisperse Flow

Table of Contents

List of Figures

Chapter 1

Introduction and Motivation

Multiphase flows are extremely important in a wide range of engineering and scientific applications. The flows of interest in this work are comprised of a large number of small particles or droplets coupled to a background fluid flow. Such flows are typical, for example, of internal combustion engines, when fuel is injected as a cloud of tiny droplets. If combustion is not efficient, tiny soot particles can be created, which are a major environmental concern. These flows also have biological applications, such as the flow from an inhaler that can be used to deliver drugs to the lungs. Another application is in emergency response evaluation from the dispersal of particles resulting from the explosion of a radiological dispersal device (RDD). The determination of the contaminated area from the deposition of particles is extremely important, especially when urban environments are considered.

Though multiphase flows of this type are important in many practical applications, all current standard models for their prediction suffer from difficulties. More specifically, Lagrangian methods can become prohibitively expensive when the number of particles becomes large. Alternatively, Eulerian methods treat multiphase flows through the definition of partial differential equations (PDEs) that govern the evolution of field variables and therefore can be more computationally affordable. However, all currently popular Eulerian methods suffer from modelling artifacts that can render them invalid in certain situations. In particular, the most common field-based models does not allow for the crossing of streams of non-interacting particles [40, 42]. This deficiency stems from the fact that traditional Eulerian models often assume that all particles at a location in space share the same velocity. New, affordable Eulerian models for multiphase flow are expected to greatly increase the range of practical situations for which such models can provide physically accurate predictions.

The situation of many weakly interacting particles of a multiphase flow has many similarities to traditional gas flows comprised of atoms or molecules. Each particle can

be assumed to follow relatively simple laws, however, the sheer number of particles precludes a direct treatment. It is therefore expected that successful and powerful techniques from the kinetic theory of gases should be adaptable to the treatment of multiphase flows. The specific techniques that will be used in this study are moment closures [16]. These closures lead to an expanded set of PDEs that describe the evolution of statistics of the distribution of particle velocities.

A different class of moment-based methods have previously been studied for the prediction of particles spreading in a turbulent background flow field [54, 33, 36, 37, 3, 46]. Though this present work is inspired by the same kinetic description of particle motion, the goal and models developed here are quite different. Rather than deriving closing relations to model the effect of unresolved turbulence in the background flow field, the present goal is to generate predictive Eulerian models for the motion of inertial particles displaying a range of velocities through a laminar background flow.

Several authors have previously investigated the application of moment closures to disperse particle movement with a background laminar flow. For example, Fox [10, 11] modelled such flows using a range of quadrature-based moment methods. More recently, Vié *et al.* made use of a ten-moment model to describe the secondary particle flow [51] and found that it leads to improved accuracy over traditional models for several simple test cases. The present study is an extension of this work.

First, an investigation of several moment-methods and demonstration of their predictive capabilities for the accurate prediction of multiphase flow is shown, specifically the models abilities to allow clean particle-stream crossing. Comparisons are made between predictions found using a traditional single-velocity model, a treatment of the particle phase using the Euler equations, the ten-moment model, and a newer fourteen-moment model.

Next, in a project with collaboration from the Canadian Nuclear Laboratory, a new moment model is developed that is based on modern techniques from the kinetic theory of gases. To goal is to model an explosive multiphase blast from a radiological dispersal devices. Flows that are typically produced by radiological dispersal devices are difficult to model efficiently. The particle phase transitions from

a dense initial phase to a highly dispersed phase later in the evolution. Particles are carried by a complex background flow that is highly compressible and contains strong shock waves. Accurately predicting the evolution of the radioactive particle phase is difficult, especially in the complex geometry of the urban environment. Traditional Eulerian methods for multiphase flow prediction all suffer from well-known modelling artifacts that render them inapplicable to this situation. In such situations, the distances over which radioactive particles are transported depend strongly on the particle sizes, as well as the background flow. A Multi-Cloud Radiological Explosive Source (MCREXS) modelling approach for RDD was explored by Ivan *et al.* [20] and obtained positive results. A new higher-order moment model based on the already popular ten-moment model is developed here and applied. The derivation, mathematical structure, and predictive capabilities of the resulting model are explored. A simple one-dimensional numerical implementation is presented and results for a flow problem that is designed to demonstrate the fundamental behaviour of the model is presented.

The remainder of this thesis is structured as follows. Chapter 2 provides a description of the multiphase flows that are of interest in this work. A kinetic description of particle motion is provided in Chapter 3. Section 3.4 explains, in detail, how the moment equations are obtained for the various models. Chapter 4 shows how to extend the traditional moment method for an application to polydisperse flows. The derivation of the new polydisperse moment model based on the existing ten-moment equations is provided in this chapter. In Section 4.2 an analysis of the new model showing proof of well-posedness is given. Next, in Chapter 5, solutions of the moment equations for the prediction of monodisperse problems are discussed. Section 5.1 describes an illustrative problem involving repeatedly crossing beams. This very difficult problem has been used previously in the literature to demonstrate the difficulty of modelling crossing particle streams using traditional Eulerian methods. Chapter 6 presents several polydisperse problems solved by using the newly proposed moment model. The first problem consists of a space homogeneous problem illustrating the evolution of the distribution function. Next, a Riemann problem is shown with a

range of drag intensities, demonstrating the numerical properties of the new model. Finally, in Chapter 7, conclusions are drawn on this research and directions of future research are outlined.

1.1 Contributions

This work conains two main contributions. Firstly, a new fourteen-moment model that has been proposed for non-equilibrium gas-flow prediction is adapted for the application to monodisperse multiphase flow. It is shown that the resulting model is able to accurately capture complex phenomena, such as particle-stream crossing. All previously proposed similar methods have failed this test. The fourteen-moment model proposed herein is demonstrated to be the lowest-order model capable of representing this behaviour.

The second main contribution of this work is the development of a new fifteen-moment model for the prediction of polydisperse particle flows. This model is an extension of the classical ten-moment model of gaskinetic theory with the ability to reporesent a continuous distribution of particle sizes. The model naturally treats statistical corelations between particle size and all other particle properties. This model is shown to greatly improve solution accuracy for several problems of interest.

Chapter 2

Multiphase Flow

Multiphase flows include a very wide range of physical situations. Each situation displays a variety of complex behaviours that bring modelling difficulties. In the first part of this study, the flow is comprised of a monodispersed spherical particle phase that is made up of solid particles or liquid droplets. In monodispersed flow, all the particles are identical, having the same diameter. In situations where the particles have different sizes the flow is said to be polydisperse. Another important characteristic of the mutiphase flow regime to define is the Knudsen number. The Knudsen number is a non dimensional number that allows one to characterize a flow regime. It shows the importance of particles collision in the particles regime. The Knudsen number, Kn, is define as

$$\mathrm{Kn} = \frac{\lambda}{\ell}\,, \tag{2.1}$$

where λ is the mean free path and ℓ is a characteristic length. In situation where Kn is small, $\mathrm{Kn} < 0.01$, the inter-particle collisions dominate, this regime is called the continuum regime. The transition regime is encountered when the Knudsen number is between 0.1 and 10. Then, with a large Knudsen number, when $\mathrm{Kn} > 10$, the flow enters the fully rarefied regime, where the collision are infrequent and can be ignored. This kind of flow is also called disperse flow. In this research, the particles are assumed to be dispersed enough so that particle interaction and particle collisions can be neglected. Such particle-laden regimes can also be characterized by the Stokes number, St, which is defined as

$$\mathrm{St} = \frac{\tau |V_i|}{\ell}\,. \tag{2.2}$$

Here, $|V_i|$ is the speed of the background fluid flow, ℓ is a characteristic length of the particle, and τ is a relaxation time that describes the rate at which differences in velocity between the particle and background flow are attenuated due to the drag force. The Stokes number is used to define how strongly the particles are affected

by drag due to the background flow. When St $\ll 1$, particle motion is strongly coupled to the carrier phase and the differences in velocity quickly becomes negligible. When St ≈ 1, particles are still affected by the background flow, but particles and the background flow can have a significant difference in velocities. When St $\gg 1$, the particles are only weakly influenced by the background fluid and tend to move ballistically.

In this research, the fluid will be assumed to follow the Stokes-flow approximation to model the flow around a particle. This Stokes law is valid for very low Reynolds number and can model the drag force between the spherical particles and the carrier phase. In this research, since the particles are small enough, this approximation is valid. The acceleration of the particle can be expressed as

$$a_i = \frac{V_i - v_i}{\tau}\,, \tag{2.3}$$

with

$$\tau = \frac{\rho_p d^2}{18\mu_f}, \tag{2.4}$$

where V_i is the background fluid velocity at the position of the particle, μ_f is the dynamic viscosity of the fluid, v_i is the particle velocity, ρ_p is the density of the material making up the particle and d is the particle diameter. Although Stokes law is only valid following the assumption of very low Reynolds numbers, more complicated models for particle drag are available at higher Reynolds numbers and would be easily applied to the situations of this work [41, 50, 17]. A more general form of the relaxation time for different drag laws can be expressed as

$$\tau_c = \frac{m_p}{3\pi d_p \mu_f}\frac{G}{f(\mathrm{Re}_p)}\,. \tag{2.5}$$

The function $f(\mathrm{Re}_p)$ is a non-linear correction for the Stokes drag approximation shown in Eq. (2.4) and G is the a correction factor known as the Cunningham correction. This non-linear correction can be expressed as

$$f(\mathrm{Re}_p) = 1 + d_1 \mathrm{Re}_p^{d_2} + \frac{\mathrm{Re}_p}{24}\frac{d_3}{1 + {}^{d_4}/_{\mathrm{Re}_p^{d_5}}}\,, \tag{2.6}$$

where the different coefficients for different drag laws are shown in Table 2.1. The

Table 2.1: Drag coefficient for five common drag laws

	d_1	d_2	d_3	d_4	d_5
Stokes [39]	0	0	0	0	0
Oseen [39]	$3/16$	1	0	0	0
Klyachko-Putnam [39]	$1/6$	$2/3$	0	0	0
Turton and Levenspiel [50]	0.173	0.657	0.413	16300	1.09
Haider and Levenspie [17]	0.1806	0.6459	0.4251	6880.95	1

Cunningham correction [39] is define as

$$G = 1 + \mathrm{Kn}\left[2.492 + 0.84\exp\left(-\frac{1.74}{\mathrm{Kn}}\right)\right]. \tag{2.7}$$

In this research, since Stokes drag is used for low Reynolds number and the Knudsen number is small, the Cunningham correction will be neglected. Using these assumption one can easily see that Eq. (2.5) can reduce to Eq. (2.4).

2.1 Traditional Treatment of Multiphase Flow

The particle phase of multiphase flow can be modelled with a Lagrangian model that tracks the trajectory of the particles individually or an Eulerian model through the form of PDEs.

In a Lagrangian model, the trajectories on which particles move are described by an ordinary differential equation. This equation for an individual particles is given by

$$m_p\frac{dv_i}{dt} = f_b + f_a + f_m + f_d + f_B\,. \tag{2.8}$$

Here, m_p is the particle mass and v_i is the velocity vector of the particle. The forces acting on the particles and shown on the right hand side of the equation are as follows: f_b is the buoyancy forces, f_a is the force due to the fluid acceleration, f_m is the forces due to the added mass, f_d is the force due to drag and f_b is the Basset history forces. The position of a certain particle can then be found by integrating

$$x_i = \int v_i dt\,, \tag{2.9}$$

where x_i is the position vector. Note that in this research the effect of gravity, buoyancy, the forces due to added mass, and the Basset history forces on the particles

motion are neglected but could easily be added. Ideally, all particles in the fluid would be tracked with ODEs, but, due to the shear number of particles, a more suitable computational approach is to track only a reduced number of variables. A more complete derivation process of Eq. (2.8) is outline by Maxey and Riley [28] and Landau and Lifshitz [24].

A typical Eulerian model for multiphase flow is the so-called single-velocity model. This model is similar to the governing Euler equations for gaseous flows without any pressure term. In contrast to the Euler equations, the single-velocity model includes only conservation equations for mass and momentum, and does not include pressure terms. The equations that describe this model with Stokes drag are

$$\frac{\partial}{\partial t}\rho + \frac{\partial}{\partial x_i}\left(\rho u_i\right) = 0\,, \tag{2.10}$$

$$\frac{\partial}{\partial t}\left(\rho u_j\right) + \frac{\partial}{\partial x_i}\left(\rho u_i u_j\right) = \frac{\rho}{\tau}(V_j - u_j)\,. \tag{2.11}$$

The single-velocity model suffers from many mathematical artifacts. In situations where the particles display a range of velocities, the modelling deficiencies become apparent, which include an inability for the model to predict crossing of particle streams and to properly apply reflective boundary conditions [40, 42]. This model can be derived as a moment closure, as shown in Section 3.4.2 and will be explained in more detail later.

Chapter 3

Traditional Kinetic Theory

3.1 Kinetic Description of Particle Motion

Treating particles individually can be computationally expensive. Instead, an Eulerian approach based on the kinetic theory of gases can be used to describe the situation of multiphase flow. In kinetic theory, particles are treated probabilistically through the definition of a distribution function. This distribution function, $\mathcal{F}(x_i, v_i, t)$, defines the number of particles in a physical cube between the points x_i and $x_i + \mathrm{d}x_i$ and with velocities between v_i and $v_i + \mathrm{d}v_i$ at a time t. In Figure 3.1, a 1D example distribution is shown. The horizontal axis shows the velocity of the particles and the vertical axis shows the density of particles with this velocity. Distribution functions can have different shapes but are always non-negative. This particular distribution function shows two groups of particles at a point in space and time. The majority of the particles have zero velocity with a small deviation and another group of particles with an average velocity of 5.0 m/s can also be seen. In the first part of this research, as in traditional kinetic theory, the distribution function does not differentiate particles of different sizes. The distribution is high dimensional—it exist in six dimensions, three space and three velocity dimensions.

3.2 Moments of the Distribution Function

Fortunately, the huge amount of information contained in the distribution function is rarely desired. Instead, traditional "macroscopic" properties are of interest. These traditional macroscopic properties are velocity moments of this distribution function. The operation of integrating the distribution function, optionally multiplied by a velocity-dependent weight, over all velocity space is called a moment of $\mathcal{F}$. For

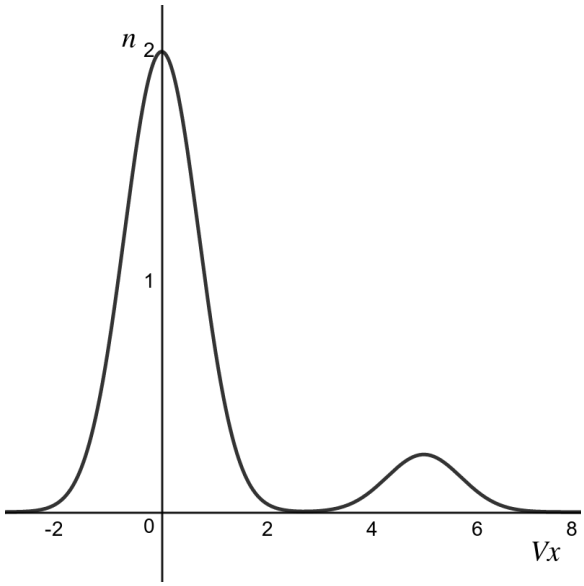

Figure 3.1: Graphical illustration of a 1D example distribution function

example, integrating this distribution in all velocity space gives to the number density,

$$n = \iiint_{\infty} \mathcal{F} \mathrm{d}v_i = \langle \mathcal{F} \rangle \ . \tag{3.1}$$

To compute higher-order moments of the distribution function, one multiplies the distribution function by a particle-velocity weight, $W(v_i)$, and again integrates over all velocity space. It is possible to obtain the mass density of the particles phase by multiplying the number density by the particle mass. The first-order moment corresponds to the momentum density of the particles. It is computed using the particle momentum as the integrating weight, as

$$\rho u_i = \langle m v_i \mathcal{F} \rangle \ . \tag{3.2}$$

It is then possible to get the average velocity of particles by

$$u_i = \frac{\langle m v_i \mathcal{F} \rangle}{\langle m \mathcal{F} \rangle} \, . \tag{3.3}$$

This allows one to define $c_i = v_i - u_i$ as the difference between an individual particle's velocity and the local average. This is also referred to as the peculiar or random

velocity [15]. Other higher-order moment of the distribution function are defined as

$$\begin{aligned} U_{ij} &= \langle m v_i v_j \mathcal{F} \rangle \ , & P_{ij} &= \langle m c_i c_j \mathcal{F} \rangle \ , \\ U_{ijk} &= \langle m v_i v_j v_k \mathcal{F} \rangle \ , & Q_{ijk} &= \langle m c_i c_j c_k \mathcal{F} \rangle \ , \\ U_{ijkl} &= \langle m v_i v_j v_k v_l \mathcal{F} \rangle \ , & R_{ijkl} &= \langle m c_i c_j c_k c_l \mathcal{F} \rangle \ , \\ U_{ijklm} &= \langle m v_i v_j v_k v_l v_m \mathcal{F} \rangle \ , & S_{ijklm} &= \langle m c_i c_j c_k c_l c_m \mathcal{F} \rangle \ . \end{aligned} \tag{3.4}$$

The "full" second-order moment, U_{ij}, is related to the kinetic energy density of the particles phase, E, through the relation

$$E = \iiint_{\infty} \frac{1}{2} m v_i v_i \, \mathcal{F} \, \mathrm{d}v_i = \frac{1}{2} U_{ii} \, . \tag{3.5}$$

The "random" second moment, P_{ij}, is related to variance-covariance tensor of particle velocities, Θ_{ij}, at a point and time through the relation

$$\Theta_{ij} = \frac{P_{ij}}{\rho} \, . \tag{3.6}$$

When modelling a gas, P_{ij} is commonly known as the pressure tensor as it is the negative of the fluid stress and describes the force that the gas would exert on an immersed surface at a particular orientation. Also for gases, Θ_{ij} is defined as the temperature tensor. The standard thermodynamic pressure of a monatomic gas is related to the trace of the pressure tensor as $p = \frac{1}{3} P_{ii}$. When describing the situation of multiphase flow, it is better to describe this higher-order moment as a statistic of the distribution of particles velocities. P_{ij} is now simply interpreted as a measure of the standard deviation of particles velocities at a location. As the order of the moment increases, the macroscopic physical meaning of its value quickly becomes less and less intuitive.

3.3 Boltzmann Equation

The evolution of this distribution function is described by the evolution equation,

$$\frac{\partial \mathcal{F}}{\partial t} + v_\alpha \frac{\partial \mathcal{F}}{\partial x_\alpha} + \frac{\partial}{\partial v_\alpha} \left(a_\alpha \mathcal{F} \right) = \frac{\delta \mathcal{F}}{\delta t} \, . \tag{3.7}$$

Again, a_α is the acceleration of a particle due to external forces. For the present study, this is the particle drag from the background fluid, as described by Eq. (2.3). The term on the right-hand side of Eq. (3.7) models the inter-particle effects, such as collisions. As the particle phase is currently assumed to be disperse, such interaction are neglected,

$$\frac{\delta \mathcal{F}}{\delta t} = 0\,. \tag{3.8}$$

In the kinetic theory of gases, where the particles of interest are the atoms or molecules, Eq. (3.7) is known as the Boltzmann equation [15, 43, 23]. In the field of multiphase flow prediction, it is more commonly known as the generalized population balance equation [27].

3.4 Moment Methods

One can obtain PDEs that govern the evolution of an arbitrary moment of the particle-phase distribution function by taking velocity moments of Eq. (3.7). Which leads to

$$\frac{\partial}{\partial t}\left\langle mW\mathcal{F}\right\rangle + \frac{\partial}{\partial x_\alpha}\left\langle mv_\alpha W\mathcal{F}\right\rangle + \left\langle mW\frac{\partial}{\partial v_\alpha}\left(a_\alpha\mathcal{F}\right)\right\rangle = 0\,. \tag{3.9}$$

This is often referred to as Maxwell's equation of change [15]. The term involving the particle acceleration can be simplified using the product rule,

$$\left\langle mW\frac{\partial(a_\alpha\mathcal{F})}{\partial v_\alpha}\right\rangle = \left\langle\frac{\partial}{\partial v_\alpha}(mWa_\alpha\mathcal{F})\right\rangle - \left\langle ma_\alpha\mathcal{F}\frac{\partial W}{\partial v_\alpha}\right\rangle\,. \tag{3.10}$$

If $\mathcal{F}$ decays to zero quickly enough as $v_i \to \infty$, the first moment on the right-hand side of Eq. (3.10) will be equal to zero. As the weight, W, is almost always taken to be a velocity monomial, its derivative is a lower-order monomial of velocity. For Stokes flow, this acceleration term can be further simplified to

$$\left\langle ma_\alpha\mathcal{F}\frac{\partial W}{\partial v_\alpha}\right\rangle = \frac{1}{\tau}\left(V_\alpha\left\langle m\mathcal{F}\frac{\partial W}{\partial v_\alpha}\right\rangle - \left\langle mv_\alpha\mathcal{F}\frac{\partial W}{\partial v_\alpha}\right\rangle\right)\,. \tag{3.11}$$

Again, V_α is the velocity of the background fluid flow. The equation for the evolution of a general moment, $U_{ij\ldots n}$, of the distribution function describing the monodisperse particle phase with Stokes drag can be expressed in balance-law form as

$$\frac{\partial}{\partial t}U_{ij\ldots n} \;+\; \frac{\partial}{\partial x_\alpha}U_{ij\ldots n\alpha} = S_{ij\ldots n}\,, \tag{3.12}$$

where $S_{ij\ldots n}$ is the source of $U_{ij\ldots n}$, predicted by Eq. (3.11).

Inspection of Eq. (3.12) immediately reveals that this technique cannot naturally lead to closed sets of equations, as the time evolution of any moment depends on the spacial divergence of a moment that is one order higher. It would therefore require an infinite number of moment equations to fully describe the evolution of a particle phase in general.

3.4.1 Moment Closures

A technique used to close the infinite series of equations provided by Eq. (3.9) is known as a moment closure. This is done by, first, defining a vector of moments that contains all the moment of interest that will act as the solution vector in the model,

$$\boldsymbol{U} = \langle m\boldsymbol{W}\mathcal{F} \rangle \ . \tag{3.13}$$

The vector, $\boldsymbol{W}$, contains all the velocity monomials that correspond to the moments in the solution vector, $\boldsymbol{U}$. In order to obtain a closed system, one restricts the distribution function, $\mathcal{F}$, to have a prescribed form. This form should be a function of a vector of unknown free parameters, $\boldsymbol{\alpha}$, that contains the same number of free parameters as unknown moments in the desired model. The free parameters are chosen such that the moment relations of Eqs. (3.3) and (3.4) are satisfied. Any higher-order moment needed to close the system can then simply be integrated and the system is closed. Once moments of interest are chosen, it is the assumed form of $\mathcal{F}$ that completely determines the properties of the closure.

3.4.2 Single-Velocity Model

One simple example of a moment closure for the prediction of particle flows has a solution vector containing mass and momentum density as unknown, $\boldsymbol{U} = [\rho, \rho u_i]^{\mathrm{T}}$. The distribution function can be selected such that all the particles at a point in space and time have the same velocity. Under this assumption, the distribution function is a Dirac delta,

$$\mathcal{F}_{\mathrm{S.V.}} = \rho \, \delta \left(v_i - u_i \right) \ . \tag{3.14}$$

The closure coefficients that make this distribution consistent with Eqs. (3.1)–(3.3) are $\boldsymbol{\alpha} = [\rho, u_i]^{\mathrm{T}}$. When this distribution function is inserted into Eq. (3.9), the resulting system of four PDEs is

$$\frac{\partial}{\partial t}\rho + \frac{\partial}{\partial x_i}\left(\rho u_i\right) = 0\,, \tag{3.15}$$

$$\frac{\partial}{\partial t}\left(\rho u_j\right) + \frac{\partial}{\partial x_i}\left(\rho u_i u_j\right) = \frac{\rho}{\tau}(V_j - u_j)\,. \tag{3.16}$$

This single-velocity model is a very common Eulerian model for the prediction of multiphase flows. This is an appropriate model for flows with very low Stokes numbers, when particle drag dominates and particles are expected to have velocities that do not deviate significantly from the background flow. However, for larges Stokes numbers, it is expected that particles will often display a range of velocities at a given point in space. In these situations, artifacts of the model become apparent, which include an inability for the model to predict crossing of particle streams and an inability to properly apply reflective boundary conditions [40, 42].

To extend this model to a range of velocities, several option are available. One can add multiple single-velocity model to create a multi-velocity or simply discrete-velocity model. Doing so, one can approximate a more complex distribution function such as a normal distribution function by regrouping particles into a sum of delta function as shown in Figure 3.2 or Eq. (3.17). In the simplest form of this model, a global set of discrete velocities is chosen and the distribution becomes

$$\mathcal{F}_{\text{S.V.}} = \sum \rho\delta\left(v_i^{\alpha} - u_i^{\alpha}\right)\,. \tag{3.17}$$

The problem with this method is that it requires as many PDEs as discrete velocities needed to accurately represent the distribution function. If not enough discretization points are used, the form and properties of the distribution function cannot be recreated, while having too many discretization points will increase computation time.

3.4.3 Quadrature-Base Method

In order to produce Eulerian models that partially overcome such limitations, one must allow the distribution function to take more general forms. There are several

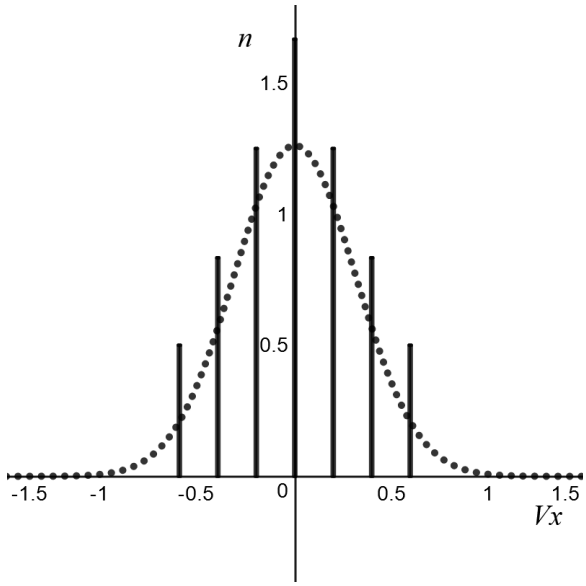

Figure 3.2: One dimensional distribution function and a multi-velocity model representation.

obvious ways to do this. One generalization leads to the Quadrature-Based Moment Methods [10, 11]. These methods allow particles to take one of a finite set of velocities at any point. This set of velocities can vary both from point to point in space as well as in time. Such quadrature-based methods have proven to be quite successful and allow for the accurate modelling of traditionally difficult behaviour. However, these methods can be somewhat difficult to implement, as the algorithms to locate the position of the delta functions that make up $\mathcal{F}$ can be numerically difficult for three-dimensional moments. Alternative methods that reduce this three-dimensional moment-inversion problem to a series of one-dimensional problems exist, however this results in a loss of rotational invariance of the models, as principal directions must be selected *a priori* [53].

3.4.4 Grad Closure Hierarchy

An alternative method for the generalization of the assumed form given in Eq. (3.14) is to replace the delta by a continuous distribution function. In the kinetic theory of gases, such moment methods have been studied for many years. It is expected that techniques originally developed for the prediction of gases can be naturally extended

to the prediction of a more general particle phase.

The first example of moment closures applied to the description of gases is due to Grad [16]. Grad's family of closures are based on an assumed distribution function that is an expansion in terms of Hermite polynomials around the local equilibrium distribution. The assumed distribution function can be expressed as

$$F_G = \mathcal{M}\left(1 + \boldsymbol{\alpha}^T \boldsymbol{H}\right) , \tag{3.18}$$

where $\mathcal{M}$ is a Maxwellian distribution function and $\boldsymbol{\alpha}$ contains N closure coefficients that are related to low-order moment. $\boldsymbol{H}$ is a vector containing Hermite polynomials. Although these closures are expressible as a closed-form first-order system of balance laws, PDEs of the model can become ill-posed. This is due to the first-order balance laws developing complex characteristics and losing hyperbolicity [48, 4, 49]. This has seriously limited the applicability of such closures.

3.4.5 Maximum-Entropy Closures

An alternative hierarchy of moment closures can be constructed by choosing $\mathcal{F}$ to be the distribution that is consistent with the moments in $\boldsymbol{U}$ while maximizing the entropy [8, 35, 25]. There are many arguments as to why a maximum-entropy assumption is an attractive choice. The most convincing of which is that the maximum-entropy state is the most likely state that is consistent with all known statistics of the particle velocities [34]. The resulting distribution functions for models in this hierarchy are of the form

$$\mathcal{F}_{\text{M.E.}} = e^{\boldsymbol{\alpha}^{\mathbf{T}} \boldsymbol{W}} . \tag{3.19}$$

Moment methods produced using this assumed form appear to have many desirable properties. For example, the distribution functions are guaranteed to be positive valued and the resulting moment equations are guaranteed to be first-order hyperbolic balance laws [35, 25]. This proof of hyperbolicity can be obtain by defining the density and flux potential as

$$h(\boldsymbol{\alpha}) = \left\langle e^{\boldsymbol{\alpha}^T \boldsymbol{W}} \right\rangle , \quad f_i(\boldsymbol{\alpha}) = \left\langle v_i e^{\boldsymbol{\alpha}^T \boldsymbol{W}} \right\rangle . \tag{3.20}$$

Then, the closure moments can be shown to be

$$\frac{\partial h}{\partial \boldsymbol{\alpha}} = \left\langle \boldsymbol{W} e^{\boldsymbol{\alpha}^T \boldsymbol{W}} \right\rangle, \quad \frac{\partial f_i}{\partial \boldsymbol{\alpha}} = \left\langle v_i \boldsymbol{W} e^{\boldsymbol{\alpha}^T V} \right\rangle. \tag{3.21}$$

The moment equation can then be written as

$$\frac{\partial}{\partial t}\frac{\partial h}{\partial \boldsymbol{\alpha}} + \nabla_i \frac{\partial f_i}{\partial \boldsymbol{\alpha}} = R(\boldsymbol{\alpha}), \tag{3.22}$$

where $R(\boldsymbol{\alpha})$ is the source term related to particles collision. The density and potential flux can then be differentiated again to give

$$h_{,\boldsymbol{\alpha}\,,\boldsymbol{\alpha}} = \frac{\partial}{\partial \boldsymbol{\alpha}}\frac{\partial h}{\partial \boldsymbol{\alpha}} = \left\langle \boldsymbol{W}[\boldsymbol{W}]^T e^{\boldsymbol{\alpha}^T \boldsymbol{W}} \right\rangle, \tag{3.23}$$

$$f_{i,\boldsymbol{\alpha}\,,\boldsymbol{\alpha}} = \frac{\partial}{\partial \boldsymbol{\alpha}}\frac{\partial f_i}{\partial \boldsymbol{\alpha}} = \left\langle v_i \boldsymbol{W}[\boldsymbol{W}]^T e^{\boldsymbol{\alpha}^T V} \right\rangle. \tag{3.24}$$

The moment equation shown above can now be expressed as

$$h_{,\boldsymbol{\alpha}\,,\boldsymbol{\alpha}} \frac{\partial \boldsymbol{\alpha}}{\partial t} + f_{i,\boldsymbol{\alpha}\,,\boldsymbol{\alpha}} \cdot \nabla_i \boldsymbol{\alpha} = R(\boldsymbol{\alpha}). \tag{3.25}$$

The time evolution and transport of the closure coefficients, $\boldsymbol{\alpha}$, for the maximum entropy distribution is shown by Eq. (3.25). The symmetry of $f_{i,\boldsymbol{\alpha}\,,\boldsymbol{\alpha}}$ and the symmetric positive definiteness of $h_{,\boldsymbol{\alpha}\,,\boldsymbol{\alpha}}$ is enough to prove the hyperbolicity of the system. The positive-definiteness of $h_{,\boldsymbol{\alpha}\,,\boldsymbol{\alpha}}$ is clear, because, for any vector $\mathbf{w}$,

$$\mathbf{w}^T h_{,\boldsymbol{\alpha}\boldsymbol{\alpha}}\, \mathbf{w} = \left\langle \mathbf{w}^T \boldsymbol{W}[\boldsymbol{W}]^T \mathbf{w} e^{\boldsymbol{\alpha}^T V} \right\rangle \geq 0, \tag{3.26}$$

and thus $h_{,\boldsymbol{\alpha}\,,\boldsymbol{\alpha}}$ is both symmetric and positive definite. Note that the transport equation from Eq. (3.25) are in the form of a Godunov symmetric hyperbolic system [14] and this can be shown to be equivalent to the classical Friedrichs-Lax form for hyperbolic system [12, 25].

The lowest-order member of the maximum-entropy hierarchy is the Euler closure. It results from the vector of generating weights $\boldsymbol{W} = [1, v_i, \frac{1}{2} v_i v_i]^{\mathrm{T}}$ and has an assumed distribution function that can be expressed as

$$\mathcal{F}_E = \frac{\rho}{m}\left(\frac{\rho}{2\pi p}\right)^{\frac{3}{2}} e^{\left(-\frac{\rho}{2p} c_i c_i\right)}. \tag{3.27}$$

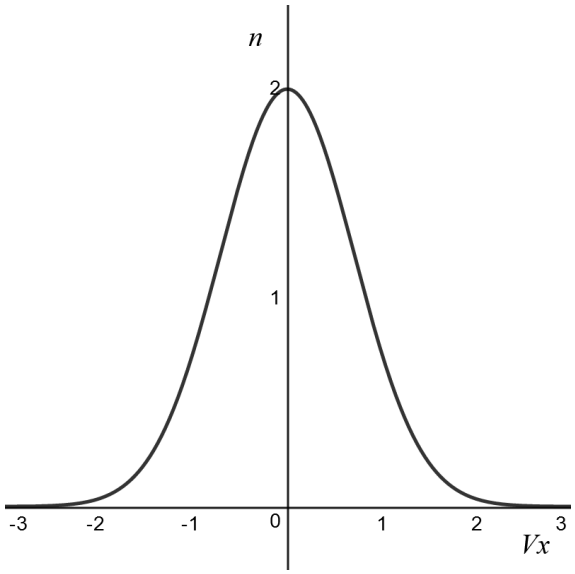

Figure 3.3: Euler particles distribution function in one dimension.

This distribution function now allows the particles to have a range of velocities at a certain point in space and time. The particle distribution function now has the shape of a normal distribution function in all velocity space directions. Figure 3.3 show an example distribution function in the x direction and Figure 3.4 show a typical 2D distribution function. This choice of distribution function leads to the moment equations,

$$\frac{\partial \rho}{\partial t} + \frac{\partial}{\partial x_i}\left(\rho u_i\right) = 0\,, \tag{3.28}$$

$$\frac{\partial}{\partial t}\left(\rho u_i\right) + \frac{\partial}{\partial x_j}\left(\rho u_i u_j + \delta_{ij} p\right) = \frac{\rho}{\tau}(V_j - u_j)\,, \tag{3.29}$$

$$\frac{\partial}{\partial t}\left(\frac{3p}{2} + \frac{\rho u_i u_i}{2}\right) + \frac{\partial}{\partial x_j}\left(u_j\left(\frac{5p}{2} + \frac{\rho u_i u_i}{2}\right)\right) = \frac{\rho u_i (V_i - u_i) - 3p}{\tau}\,. \tag{3.30}$$

Here, δ_{ij} is the Kronecker delta. The left-hand side of these PDEs are exactly the same as the traditional Euler equations for a compressible monatomic perfect gas with $\gamma = \frac{5}{3}$, while terms related to particle drag are present on the right-hand [7, 9].

The next model in the maximum-entropy hierarchy is a ten-moment closure that uses $\boldsymbol{W} = [1, v_i, v_i v_j]^{\mathrm{T}}$ as generating weights. The resulting distribution function has the form

$$\mathcal{F}_G = \frac{\rho}{m(2\pi)^{3/2}(\det \Theta_{ij})^{1/2}} e^{\left(-\frac{1}{2}\Theta_{ij}^{-1} c_i c_j\right)}\,. \tag{3.31}$$

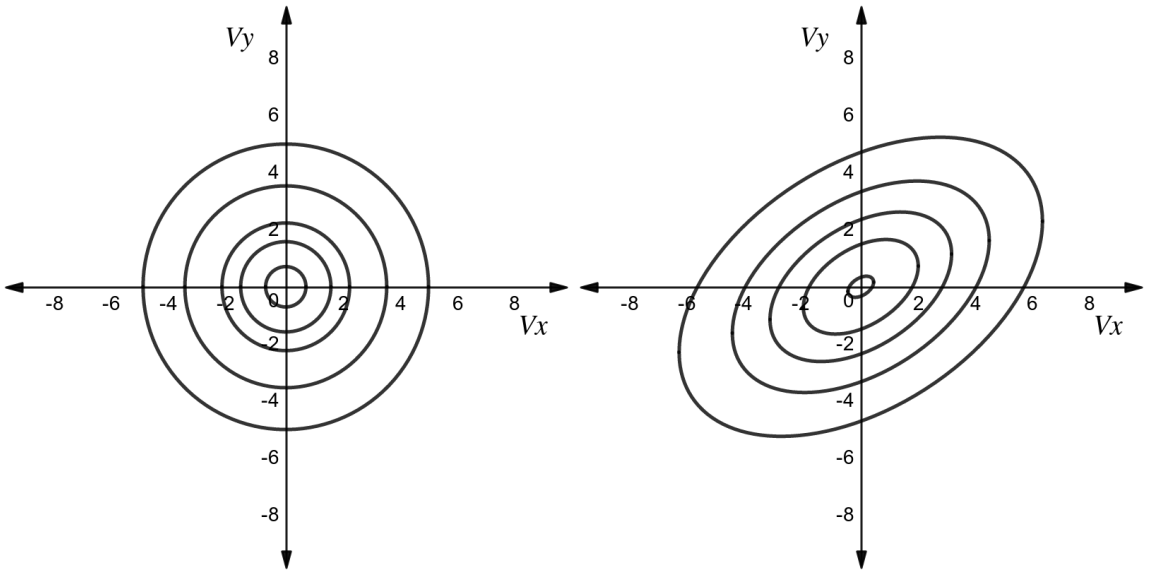

Figure 3.4: Euler distribution function on the left, ten-moment distribution function on the right in the x- and y-direction velocity space.

This distribution can be interpreted as a normal distribution with a different standard deviation for each direction. The difference between the ten-moment distribution function and the previous member of the maximum entropy hierarchy is illustrated in Figure 3.4. One can see that the standard deviation of particle velocities in this model is different in different directions. This choice leads to ten first-order hyperbolic PDEs of the form

$$\frac{\partial \rho}{\partial t} + \frac{\partial}{\partial x_k}\left(\rho u_k\right) = 0\,, \tag{3.32}$$

$$\frac{\partial}{\partial t}(\rho u_i) + \frac{\partial}{\partial x_k}(\rho u_i u_k + P_{ik}) = \frac{\rho}{\tau}(V_j - u_j)\,, \tag{3.33}$$

$$\begin{aligned}\frac{\partial}{\partial t}\left(P_{ij} + \rho u_i u_j\right) + \frac{\partial}{\partial x_k}\left(\rho u_i u_j u_k + u_i P_{jk} + u_j P_{ik} + u_k P_{ij}\right) = \\ \frac{\rho u_i (V_j - u_j) + \rho u_j (V_i - u_i) - 2P_{ij}}{\tau}\,.\end{aligned} \tag{3.34}$$

This ten-moment model has previously proven successful in modelling a wide range of equilibrium and non-equilibrium gas flows [26, 6, 5, 29, 30, 2, 45]. Recently, Vié *et al.* made use of this ten-moment model to also describe a secondary particle flow [51]. It was found that it improved predictions as compared to classical models, however it was not able to predict clean crossing of two beams of non-interacting particles. This is not surprising, given that the assumed distribution function, Eq. (3.31), is

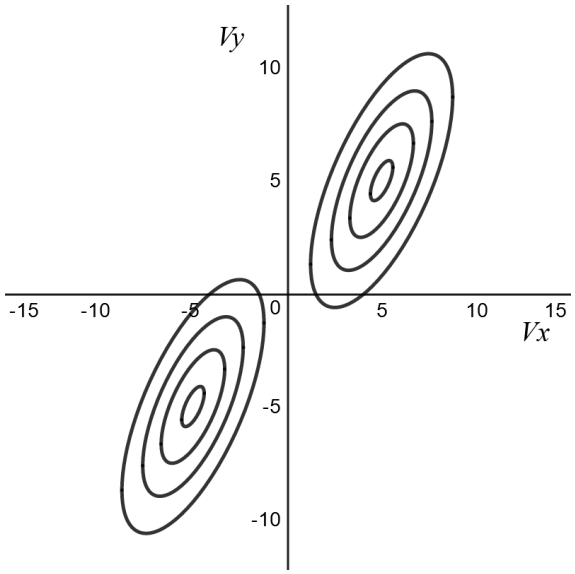

Figure 3.5: Graphical illustration of the fourteen-moment particles distribution function in the x- and y-direction velocity space.

uni-modal. At the point of crossing of two beams, a bi-modal distribution function is needed to properly represent the two distinct velocities of particle belonging to the two beams.

The next closure in the maximum-entropy hierarchy is a fourteen-moment model. It is produced using the velocity weight vector $\boldsymbol{W} = [1, v_i, v_i v_j, v_i v_j v_j, v_i v_i v_j v_j]^{\mathrm{T}}$ and contains ρ, u_i, P_{ij}, Q_{ijj}, and R_{iijj} as unknown moments in the solution vector. These generating weights produce a quartic polynomial in the exponent of Eq. (3.19). The distribution function is therefore allowed to be bi-modal. A typical distribution function is illustrated in Figure 3.5. In fact, the situations of two Dirac deltas are included as a limiting case. The resulting moment equations are

$$\frac{\partial \rho}{\partial t} + \frac{\partial}{\partial x_i}\left(\rho u_i\right) = 0\,, \tag{3.35}$$

$$\frac{\partial}{\partial t}\left(\rho u_i\right) + \frac{\partial}{\partial x_j}\left(\rho u_j u_i + P_{ij}\right) = \frac{\rho}{\tau}(V_j - u_j)\,, \tag{3.36}$$

$$\begin{aligned}\frac{\partial}{\partial t}\left(\rho u_i u_j + P_{ij}\right) + \frac{\partial}{\partial x_k}(\rho u_j u_i u_k + P_{jk}u_i + u_j P_{ik} + u_k P_{ij} + Q_{ijk}) = \\ \frac{\rho u_i(V_j - u_j) + \rho u_j(V_i - u_i) - 2P_{ij}}{\tau}\,,\end{aligned} \tag{3.37}$$

$$\frac{\partial}{\partial t}\left(\rho u_i u_j u_j + u_i P_{jj} + 2u_j P_{ij} + Q_{ijj}\right) +$$
$$\frac{\partial}{\partial x_k}(\rho u_i u_k u_j u_j + P_{jj} u_i u_k + 2u_i u_j P_{jk} + 2u_j u_k P_{ij} +$$
$$u_j u_j P_{ik} + u_i Q_{kjj} + u_k Q_{ijj} + 2u_j Q_{ijk} + R_{ikjj}) =$$
$$\frac{(V_i - u_i)(\rho u_j u_j + P_{jj}) + 2(V_j - u_j)(\rho u_i u_j + P_{ij}) - 2u_i P_{jj} - 4u_j P_{ij} - 3Q_{ijj}}{\tau}, \quad (3.38)$$

$$\frac{\partial}{\partial t}(\rho u_i u_i u_j u_j + 2u_i u_i P_{jj} + 4u_i u_j P_{ij} + 4u_i Q_{ijj} + R_{iijj}) +$$
$$\frac{\partial}{\partial x_k}(\rho u_k u_i u_i u_j u_j + 2u_k u_i u_i P_{jj} + 4u_i u_i u_j P_{jk} + 4u_i u_j u_k P_{ij} + 2u_i u_i Q_{kjj}$$
$$+4u_i u_k Q_{ijj} + 4u_i u_j Q_{ijk} + 4u_i R_{ikjj} + u_k R_{iijj} + S_{kiijj}) =$$
$$\frac{4}{\tau}\big[(V_i - u_i)(\rho u_i u_j u_j + u_i P_{jj} + 2u_j P_{ij} + Q_{ijj})$$
$$-u_i u_i P_{jj} - 2u_i u_j P_{ij} - 3u_i Q_{ijj} - R_{iijj}\big]. \quad (3.39)$$

In these expressions, the moments Q_{ijk}, R_{ijkk}, and S_{ijjkk} are not present in the solution vector and must be determined through the assumed form of the distribution function.

On first glance, this appears to be a very promising model that has the potential to accurately predict particle-stream crossing. However, there are two well-known issues related to this model. Firstly, once super-quadratic monomials are used as generating weights, moments of the distribution function, Eq. (3.19), cannot be evaluated in closed form for all moment states. The result is that the closure coefficients cannot be related to moment quantities and fluxes cannot be expressed as closed-form functions of known moments. Numerically expensive, ill-conditioned iterative techniques must be used each time a flux is required.

Yet more devastating is the fact that there exist physically realistic moment states for which no distribution function of the form given in Eq. (3.19) exists [21, 22]. This results in a breakdown of the entire framework on which the maximum-entropy theory is built. Even solutions to Eqs. (3.35)–(3.39) that do not enter the region of breakdown can be numerically difficult. This is because, as the region of closure breakdown is approached, closing fluxes become singular. Hauck *et al.* have carried out a detailed geometric analysis of the space of moment states for which a maximum-entropy distribution does not exist [19].

Recently, M$^{\text{c}}$Donald and Torrilhon have found that both of these issues can be circumvented in practice for the fourteen-moment case [31]. They did this by identifying moment states for which Eq. (3.19) can be integrated in closed form. They then proposed interpolation functions between these states. The resulting model agrees with the maximum-entropy model whenever integration of $\mathcal{F}_{\text{M.E.}}$ is possible and closing fluxes remain very close to those predicted by the true maximum-entropy distribution elsewhere.

In producing their interpolative approximations, M$^{\text{c}}$Donald and Torrilhon made use of a parabolic mapping to replace the moment variable R_{iijj} with a newly defined variable, σ, such that

$$R_{iijj} = \frac{1}{\sigma} Q_{kii} (P^{-1})_{kl} Q_{ljj} + \frac{2(1-\sigma) P_{ji} P_{ij} + P_{ii} P_{jj}}{\rho} \,. \tag{3.40}$$

The new parameter, σ, varies between zero and one for all physically possible states. A value of $\sigma = 0$ corresponds with the region of moment space for which a maximum-entropy distribution function does not exist, while a value of $\sigma = 1$ corresponds to the limits of physically realizable states.

The missing closing fluxes (Q_{ijk}, R_{ijkk}, and S_{ijjkk}) in Eqs. (3.35)–(3.39) are proposed to be

$$Q_{ijk} = K_{ijkm} Q_{mnn} \,, \tag{3.41}$$

$$R_{ijkk} = \frac{1}{\sigma} Q_{ijl} \left(P^{-1}\right)_{lm} Q_{mkk} + \frac{2(1-\sigma) P_{ik} P_{kj} + P_{ij} P_{kk}}{\rho} \,, \tag{3.42}$$

$$S_{ijjkk} = \frac{1}{\sigma^2} P^{-1}_{kn} P^{-1}_{lm} Q_{npp} Q_{mjj} Q_{ikl} + 2\sigma^{\frac{1}{2}} \frac{P_{jj} Q_{ikk}}{\rho} + (1 - \sigma^{\frac{1}{2}}) W_{im} Q_{mnn} \,, \tag{3.43}$$

with

$$K_{ijkm} = \left[2P_{il}(P^2)_{jk} + 2P_{kl}(P^2)_{ij} + 2P_{jl}(P^2)_{ik}\right] B^{-1}_{lm} \,, \tag{3.44}$$

and

$$\begin{aligned} W_{im} = \big[2P_{il}(P_{\alpha\alpha})^3 + 12P_{il}(P^3)_{\alpha\alpha} + 14(P^2)_{\alpha\alpha}(P^2)_{il} + 20P_{\alpha\alpha}(P^3)_{il} \\ + 20(P^4)_{il} - 2(P^2)_{\alpha\alpha} P_{\beta\beta} P_{il} - 6(P_{\alpha\alpha})^2 (P^2)_{il}\big] B^{-1}_{lm} \,, \end{aligned} \tag{3.45}$$

$$B_{lm} = 2P_{lm}(P^2)_{\alpha\alpha} + 4(P^3)_{lm} \,. \tag{3.46}$$

Note that the sigma in the second term of the right-hand side of Eq. (3.43) was originally raised to the power three fifths [31], however, subsequent studies have found that superior results are obtained with a value of one half [47, 32]. These fluxes maintain the singular nature of the maximum-entropy closure as the space where $\sigma = 0$ is approached. This is inconvenient numerically, but has been found to greatly improve solutions for several gas-dynamic problems [31, 47].

It should be noted that there exist several other modern moment-closure techniques in the field of kinetic theory of gases. These include the hierarchy of regularized moment closures of Struchtrup and Torrilhon [44] and the φ-divergence closures of Abdelmalik and van Brummelen [1]. Extensions of these methods to the prediction of multiphase particle-flow prediction is also possible, but are not considered here.

3.5 Reduction of the Moment Models to One Dimension

In some situation it is better to solve the model in one dimension. The single-velocity model for these situation is described by two scalar moment equations,

$$\frac{\partial}{\partial t}\rho + \frac{\partial}{\partial x}\left(\rho u\right) = 0\,, \tag{3.47}$$

$$\frac{\partial}{\partial t}\left(\rho u\right) + \frac{\partial}{\partial x}\left(\rho u^2\right) = \frac{\rho}{\tau}(V - u)\,, \tag{3.48}$$

where V is the scalar x-direction velocity of the background flow. The five-moment Euler model is reduce to three moment equations

$$\frac{\partial \rho}{\partial t} + \frac{\partial}{\partial x}\left(\rho u\right) = 0\,, \tag{3.49}$$

$$\frac{\partial}{\partial t}(\rho u) + \frac{\partial}{\partial x}(\rho u^2 + p) = \frac{\rho}{\tau}(V - u)\,, \tag{3.50}$$

$$\frac{\partial}{\partial t}\left(\frac{3p}{2} + \frac{\rho u^2}{2}\right) + \frac{\partial}{\partial x}\left(\frac{\rho u^3}{2} + \frac{5up}{2}\right) = \frac{\rho u(V - u) - 3p}{\tau}\,. \tag{3.51}$$

For the one-dimensional flow considered here, the ten-moment equations reduce to a system of three scalar equations

$$\frac{\partial \rho}{\partial t} + \frac{\partial}{\partial x}(\rho u) = 0\,, \tag{3.52}$$

$$\frac{\partial}{\partial t}(\rho u) + \frac{\partial}{\partial x}(\rho u^2 + p) = \frac{\rho}{\tau}(V - u)\,, \tag{3.53}$$

$$\frac{\partial}{\partial t}\left(p + \rho u^2\right) + \frac{\partial}{\partial x}\left(\rho u^3 + 3up\right) = \frac{2\rho u(V-u) - 2p}{\tau}\,. \tag{3.54}$$

For this one-dimensional situation, the fourteen-moment model reduces to five scalar PDEs,

$$\frac{\partial \rho}{\partial t} + \frac{\partial}{\partial x}(\rho u) = 0\,, \tag{3.55}$$

$$\frac{\partial}{\partial t}(\rho u) + \frac{\partial}{\partial x}\left(\rho u^2 + p\right) = \frac{\rho}{\tau}(V - u)\,, \tag{3.56}$$

$$\frac{\partial}{\partial t}\left(\rho u^2 + p\right) + \frac{\partial}{\partial x}\left(\rho u^3 + 3up + q\right) = \frac{2\rho u(V-u) - 2p}{\tau}\,, \tag{3.57}$$

$$\begin{aligned}\frac{\partial}{\partial t}\left(\rho u^3 + 3up + q\right) + \frac{\partial}{\partial x}\left(\rho u^4 + 6u^2 p + 4uq + r\right)\\ = \frac{3[(V-u)(\rho u^2 + p) - 2up - q]}{\tau}\,,\end{aligned} \tag{3.58}$$

$$\begin{aligned}\frac{\partial}{\partial t}\left(\rho u^4 + 6u^2 p + 4uq + r\right) + \frac{\partial}{\partial x}\left(\rho u^5 + 10u^3 p + 10u^2 q + 5ur + s\right)\\ = \frac{4[(V-u)(\rho u^3 + 3up + q) - 3u^2 p - 3uq - r]}{\tau}\,.\end{aligned} \tag{3.59}$$

The only unknown closing flux is now the scalar fifth moment, s. The definition of σ for this setting simplifies to

$$r = \frac{1}{\sigma}\frac{q^2}{p} + (3 - 2\sigma)\frac{p^2}{\rho}\,, \tag{3.60}$$

and the proposed expression for the closing flux reduces to

$$s = \frac{1}{\sigma^2}\frac{q^3}{p^2} + \frac{p}{\rho}\left(10 - 8\sigma^{\frac{1}{2}}\right) q\,. \tag{3.61}$$

Chapter 4

Polydisperse Gaussian Model

The moment methods described in Chapter 3 are well suited for application to monodisperse flows. Computations to demonstrate this fact are included in Section 5.3. It would be of great interest to explore how moment methods could be used in situation where particles have different sizes. In situation such as the dispersal of particles resulting from the explosion of a radiological dispersal device (RDD), where the particle phase at a certain locations displays a range of velocities and particle sizes, monodisperse model such as the ten-moment equation are no longer applicable. An extension to the ten-moment equation is therefore proposed to allow the particles to have a range of sizes, characterized in terms of a diameter. This is done by redefining $\mathcal{F}$ to now be a distribution function in physical space, x_i, velocity space, v_i, time, t, and diameter space, d. The evaluation of

$$\mathcal{F}(x_i, v_i, t, d)\,\mathrm{d}x_i\,\mathrm{d}v_i\,\mathrm{d}d$$

is defined to be the number of particles within a differential cube of size $\mathrm{d}x_i$ around the point x_i with a velocity within a cube of size $\mathrm{d}v_i$ of particle velocity, v_i, with a diameter within a differential distance, $\mathrm{d}d$, of d, at time t. A more general form of Eq. (3.7) for particles with a range of diameter is shown as

$$\frac{\partial \mathcal{F}}{\partial t} + v_i \frac{\partial \mathcal{F}}{\partial x_i} + \frac{\partial a_i \mathcal{F}}{\partial v_i} + \frac{\partial \phi \mathcal{F}}{\partial d} = \frac{\delta \mathcal{F}}{\delta t}\,. \tag{4.1}$$

Where the new term on the left-hand side is related to the particle's change of diameter with time. This kinetic equation is known as the Boltzmann-Williams equation [52] and is widely used in fuel-spray modelling. Even though particles are now able to posses a range of diameters, as long as each particle has a diameter that does not itself change with time, Eq. (3.7) still governs the evolution of the distribution function through phase space. The only significant difference is that the acceleration due to drag, a_i, becomes a function of the individual particle diameter. Again, the acceleration is assumed to be given by Eq. (2.3).

Another option to extend a monodisperse model to a range of diameters, is to follow the same approach as the one employed to extend the single-velocity model to a range of velocities. Such a procedure results in a discrete-velocity model which has a form given by Eq. (3.17). In the case of polydisperse flows, a similar approach would be applied to a diameter space instead. One can add multiple monodisperse models to create a discrete-diameter model. Doing so, one can approximate a more complex distribution function such as a normal or a log normal distribution function by re-grouping particles into a sum of delta function or monodisperse distribution function. Unfortunately, a large number of PDEs would be required for such a treatment.

4.1 Extensions of the Ten-Moment Model for a Distribution of Particle Sizes

To extend the ten-moment model to situations where the size of the particles vary, a new model can be created by extending the space of $\mathcal{F}$ to include a diameter space, as was shown in Eq. (4). Experiments and previous work for RDD show that the particles diameters are expected to follow a log-normal distribution [20]. Therefore, assuming a log-normal distribution for the particle size, the solution vector from the traditional ten-moment model is supplemented with moments that give information regarding the local average logarithm of the diameter of particles, μ, the local variance of the logarithm of particle diameters, Ψ_{dd}, and the covariance of particle logarithm diameter with each component of the particle velocity, Ψ_{id}. This covariance information proves to be very important, as the velocity of a particle in a background flow is expected to be heavily dependent on its size. The resulting proposed distribution function has a form similar to Eq. (3.31) and can be expressed as

$$\mathcal{F} = \frac{n}{d(2\pi)^2(\det \Psi_{ij})^{1/2}} e^{\left(-\frac{1}{2}\Psi_{ij}^{-1}\tilde{c}_i\tilde{c}_j\right)} . \tag{4.2}$$

The augmented random vector, $\tilde{c}_i$, and second-order tensor, Ψ_{ij}, are now defined as

$$\tilde{c}_i = \begin{bmatrix} v_x - u_x \\ v_y - u_y \\ v_z - u_z \\ \ln(d) - \mu \end{bmatrix} , \tag{4.3}$$

$$\Psi_{ij} = \begin{bmatrix} \Theta_{xx} & \Theta_{xy} & \Theta_{xz} & \Psi_{xd} \\ \Theta_{xy} & \Theta_{yy} & \Theta_{yz} & \Psi_{yd} \\ \Theta_{xz} & \Theta_{yz} & \Theta_{zz} & \Psi_{zd} \\ \Psi_{xd} & \Psi_{yd} & \Psi_{zd} & \Psi_{dd} \end{bmatrix} . \tag{4.4}$$

The new entry in the random vector $\tilde{c}_i$ shows the difference between the natural logarithm of the particle diameter and the local average of the logarithm of the diameter, μ. From this distribution function, the average particle diameter can be computed as

$$D = e^{\mu + \frac{1}{2}\Psi_{dd}} . \tag{4.5}$$

The variance-covariance matrix, Θ_{ij}, has now been supplemented with new entries. Here, Ψ_{id} is the covariance between the logarithm of the diameter of the particle and the velocity,

$$\Psi_{id} = \frac{1}{n} \left\langle (v_i - u_i)(ln(d) - \mu)F \right\rangle , \tag{4.6}$$

while Ψ_{dd} is the variance of the logarithm of the particle diameter

$$\Psi_{dd} = \frac{1}{n} \left\langle (ln(d) - \mu)^2 F \right\rangle . \tag{4.7}$$

These are related to the covariance between the diameter of the particle and the velocity, Θ_{id} and the variance in diameter, Θ_{dd} as

$$\Theta_{id} = \Psi_{id} D , \tag{4.8}$$

$$\Theta_{dd} = D^2 \left(e^{\Psi_{dd}} - 1 \right) . \tag{4.9}$$

Two examples of slices of the assumed form for the distribution functions in $v_x - d$ space are shown in Figures 4.1 and 4.2. In the first figure, the particles have an average velocity of $u_x = 5\,\mathrm{m/s}$, a variance in particle velocity of $\Theta_{xx} = 1.0\,\mathrm{m^2/s^2}$, average particle diameter of $D = 28.0\,\mu\mathrm{m}$, variance in particle diameter of $\Theta_{dd} = 2.2 \times 10^{-10}\,\mathrm{m^2}$ and $v_x - d$ covariance of $\Theta_{xd} = 0\,\mathrm{m^2/s}$. One can see that the distribution is log-normal in diameter space and the statistics of particle velocity is independent of the diameter.

Figure 4.2 shows the distribution function with all the same properties, except it now has a covariance between particle velocity and diameter of $\Theta_{xd} = 1.0 \times 10^{-5}\,\mathrm{m^2/s}$. One can now see that, even though the total averages are the same, the smaller

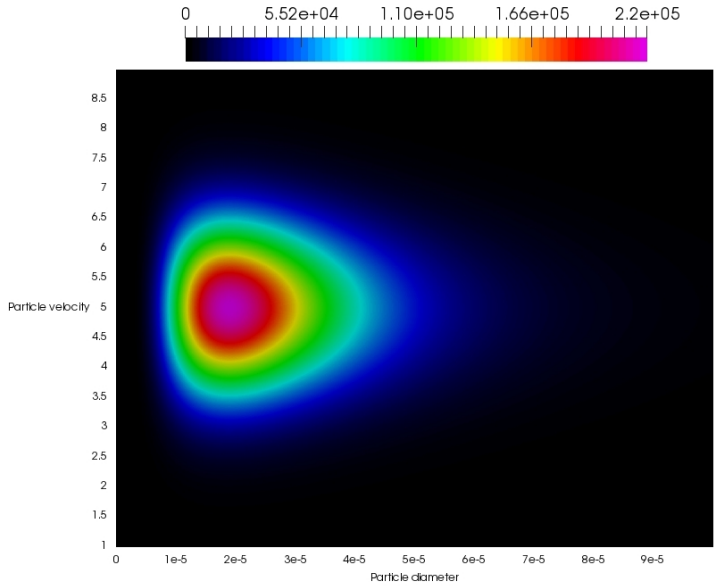

Figure 4.1: Distribution function corresponding to an average particle velocity of $5.0\,\mathrm{m/s}$, an average diameter of $28.0\,\mu\mathrm{m}$, a variance in diameter of $2.2 \times 10^{-10}\,\mathrm{m}^2$ and a variance in x-direction velocity of $1.0\,\mathrm{m}^2/\mathrm{s}^2$.

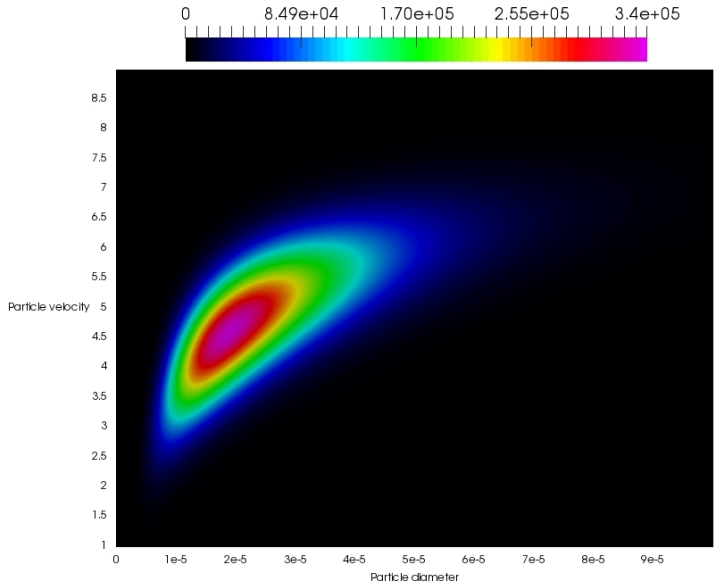

Figure 4.2: Distribution function corresponding to an average particle velocity of $5.0\,\mathrm{m/s}$, an average diameter of $28.0\,\mu\mathrm{m}$, a variance in diameter of $2.2 \times 10^{-10}\,\mathrm{m}^2$, a variance in x-direction velocity of $1.0\,\mathrm{m}^2/\mathrm{s}^2$ and a covariance of $1.0 \times 10^{-5}\,\mathrm{m}^2/\mathrm{s}$.

particles have lower speed than the larger particles. Such situations are expected to be very common of particle flows that enter a slower background flow, as the smaller particles will be decelerated by drag much more quickly than the larger particles.

With the extension of the model to include variable particle diameter, the first ten equations of the resulting moment model are modified only in the source term—the left-hand side remains unchanged. Five new PDEs are added to track information related to particle diameter. Two methods of adding entries to the solution vector have been investigated. The first model tracks statistics related directly to particle diameters, the second model tracks information related to the logarithm of particle diameters. These choices lead to slightly different models.

4.1.1 Equations Based on Average Particle Diameter

The first model investigated uses an extension that directly tracks statistics of the distribution of particle diameters. This model uses the distribution function shown in Eq (4.2) and moment-generating vector, $\boldsymbol{W} = [1, v_i, v_i v_j, d, dv_i, d^2]^{\mathrm{T}}$. This leads to a new system of fifteen first-order hyperbolic PDEs of the form of Eq. (4.14) where $\boldsymbol{U}$, the solution vector of conserved variable, and $\boldsymbol{F}_x$, the flux in the x-direction, are given by

$$\boldsymbol{U} = \begin{bmatrix} n \\ nu_x \\ nu_y \\ nu_z \\ n(u_x^2 + \Theta_{xx}) \\ n(u_x u_y + \Theta_{xy}) \\ n(u_x u_z + \Theta_{xz}) \\ n(u_y^2 + \Theta_{yy}) \\ n(u_y u_z + \Theta_{yz}) \\ n(u_z^2 + \Theta_{zz}) \\ nD \\ n(Du_x + \Theta_{xd}) \\ n(Du_y + \Theta_{yd}) \\ n(Du_z + \Theta_{zd}) \\ n(D^2 + \Theta_{dd}) \end{bmatrix} \quad \boldsymbol{F}_x = \begin{bmatrix} nu_x \\ n(u_x^2 + \Theta_{xx}) \\ n(u_x u_y + \Theta_{xy}) \\ n(u_x u_z + \Theta_{xz}) \\ n(u_x^3 + 3u_x\Theta_{xx}) \\ n(u_x^2 u_y + 2u_x\Theta_{xy} + u_y\Theta_{xx}) \\ n(u_x^2 u_z + 2u_x\Theta_{xz} + u_z\Theta_{xx}) \\ n(u_x u_y^2 + u_x\Theta_{yy} + 2u_y\Theta_{xy}) \\ n(u_x u_y u_z + u_x\Theta_{yz} + u_y\Theta_{xz} + u_z\Theta_{xy}) \\ n(u_x u_z^2 + u_x\Theta_{zz} + 2u_z\Theta_{xz}) \\ n(Du_x + \Theta_{xd}) \\ n(Du_x^2 + 2u_x\Theta_{xd} + \frac{\Theta_{xd}^2}{D} + D\Theta_{xx}) \\ n(Du_x u_y + u_x\Theta_{yd} + u_y\Theta_{xd} + \frac{\Theta_{xd}\Theta_{yd}}{D} + D\Theta_{xy}) \\ n(Du_x u_z + u_x\Theta_{zd} + u_z\Theta_{xd} + \frac{\Theta_{xd}\Theta_{zd}}{D} + D\Theta_{xz}) \\ n(D^2 + \Theta_{dd})(u_x + \frac{2\Theta_{xd}}{D}) \end{bmatrix}. \tag{4.10}$$

$\boldsymbol{F}_y$ and $\boldsymbol{F}_z$ are symmetrical to $\boldsymbol{F}_x$. The source vector for Stokes flow, $\boldsymbol{S}$, is expressed as

$$\boldsymbol{S} = \frac{1}{\tau_d}\begin{bmatrix} 0 \\ \left(nV_x - nu_x + 2\frac{\Theta_{xd}}{D}\right) \\ \left(nV_y - nu_y + 2\frac{\Theta_{yd}}{D}\right) \\ \left(nV_z - nu_y + 2\frac{\Theta_{zd}}{D}\right) \\ 2\left(V_x(nu_x - 2\frac{\Theta_{xd}}{D}) - (nu_x^2 - 4u_x\frac{\Theta_{xd}}{D} + 4\frac{\Theta_{xd}^2}{nD^2} + \Theta_{xx})\right) \\ \left(V_x(nu_y - 2\frac{\Theta_{xd}}{D}) + V_y(nu_x - 2\frac{\Theta_{xd}}{D}) - 2(nu_xu_y - 2u_x\frac{\Theta_{yd}}{D} - 2u_y\frac{\Theta_{xd}}{D} + 4\frac{\Theta_{xd}\Theta_{yd}}{nD^2} + \Theta_{xy})\right) \\ \left(V_x(nu_z - 2\frac{\Theta_{xd}}{D}) + V_z(nu_x - 2\frac{\Theta_{xd}}{D}) - 2(nu_xu_z - 2u_x\frac{\Theta_{zd}}{D} - 2u_z\frac{\Theta_{xd}}{D} + 4\frac{\Theta_{xd}\Theta_{zd}}{nD^2} + \Theta_{xz})\right) \\ 2\left(V_y(nu_y - 2\frac{\Theta_{yd}}{D}) - (nu_y^2 - 4u_y\frac{\Theta_{yd}}{D} + 4\frac{\Theta_{yd}^2}{nD^2} + \Theta_{yy})\right) \\ \left(V_y(nu_z - 2\frac{\Theta_{yd}}{D}) + V_z(nu_y - 2\frac{\Theta_{yd}}{D}) - 2(nu_yu_z - 2u_y\frac{\Theta_{zd}}{D} - 2u_z\frac{\Theta_{yd}}{D} + 4\frac{\Theta_{yd}\Theta_{zd}}{nD^2} + \Theta_{yz})\right) \\ 2\left(V_z(nu_z - 2\frac{\Theta_{zd}}{D}) - (nu_z^2 - 4u_z\frac{\Theta_{zd}}{D} + 4\frac{\Theta_{zd}^2}{nD^2} + \Theta_{zz})\right) \\ 0 \\ \left(nV_x - (nu_x - \frac{\Theta_{xd}}{D})\right) \\ \left(nV_y - (nu_y - \frac{\Theta_{yd}}{D})\right) \\ \left(nV_z - (nu_z - \frac{\Theta_{zd}}{D})\right) \\ 0 \end{bmatrix}. \tag{4.11}$$

where

$$\tau_d = \frac{\rho_p}{18\mu_f}\frac{D^8}{(\Theta_{dd} + D^2)^3} \tag{4.12}$$

The eigenvalues of the x-direction flux Jacobian are

$$\lambda_{1-15} = \begin{pmatrix} u_x + 2\frac{\Theta_{xd}}{d} \\ u_x + \frac{\Theta_{xd}}{d} + \sqrt{\Theta_{xx}} \\ u_x + \frac{\Theta_{xd}}{d} - \sqrt{\Theta_{xx}} \\ u_x + \sqrt{3\Theta_{xx}} \\ u_x - \sqrt{3\Theta_{xx}} \\ u_x + \Theta_{xd} \\ u_x + \Theta_{xd} \\ u_x + \sqrt{\Theta_{xx}} \\ u_x - \sqrt{\Theta_{xx}} \\ u_x + \sqrt{\Theta_{xx}} \\ u_x - \sqrt{\Theta_{xx}} \\ u_x \\ u_x \\ u_x \\ u_x \end{pmatrix}. \tag{4.13}$$

These represent the wave speeds defining information propagation in the PDEs. Ten of the eigenvalues are identical to the base ten-moment model, while five new eigenvalues that correspond to particle-size information propagation have appeared.

4.1.2 Equations Based on Average logarithm of the Particle Diameter

It may seem more natural to write equations in terms of the average particle diameter, rather than the logarithm of diameter, however, there are compelling reasons to believe that this second model will be more successful. This is because the resulting moment equations take on a mathematically cleaner form when the generating weights present in $\boldsymbol{W}$ correspond directly to the entries in the polynomial that is present in the exponential of Eq (4.2).

The Polydisperse Gaussian model investigated uses an extension that tracks statistics of the distribution of the logarithm of particle diameter. This model uses the distribution function shown in Eq (4.2). The generating weights are now chosen to be $\boldsymbol{W} = [1, v_i, v_i v_j, \ln(d), \ln(d) v_i, \ln(d)^2]^{\mathrm{T}}$. This leads to a new system of fifteen first-order hyperbolic PDEs of the form of

$$\frac{\partial \boldsymbol{U}}{\partial t} + \frac{\partial \boldsymbol{F}_x}{\partial x} + \frac{\partial \boldsymbol{F}_y}{\partial y} + \frac{\partial \boldsymbol{F}_z}{\partial z} = \boldsymbol{S}\,, \tag{4.14}$$

where $\boldsymbol{U}$, the solution vector of conserved variable, and $\boldsymbol{F}_x$, the flux in the x-direction, are given by

$$\boldsymbol{U} = \begin{bmatrix} n \\ nu_x \\ vu_y \\ nu_z \\ n(u_x^2 + \Theta_{xx}) \\ n(u_x u_y + \Theta_{xy}) \\ n(u_x u_z + \Theta_{xz}) \\ n(u_y^2 + \Theta_{yy}) \\ n(u_y u_z + \Theta_{yz}) \\ n(u_z^2 + \Theta_{zz}) \\ n\mu \\ n(\mu u_x + \Psi_{xd}) \\ n(\mu u_y + \Psi_{yd}) \\ n(\mu u_z + \Psi_{zd}) \\ n(\mu^2 + \Psi_{dd}) \end{bmatrix} \qquad \boldsymbol{F}_x = \begin{bmatrix} nu_x \\ n(u_x^2 + \Theta_{xx}) \\ n(u_x u_y + \Theta_{xy}) \\ n(u_x u_z + \Theta_{xz}) \\ n(u_x^3 + 3u_x\Theta_{xx}) \\ n(u_x^2 u_y + 2u_x\Theta_{xy} + u_y\Theta_{xx}) \\ n(u_x^2 u_z + 2u_x\Theta_{xz} + u_z\Theta_{xx}) \\ n(u_x u_y^2 + u_x\Theta_{yy} + 2u_y\Theta_{xy}) \\ n(u_x u_y u_z + u_x\Theta_{yz} + u_y\Theta_{xz} + u_z\Theta_{xy}) \\ n(u_x u_z^2 + u_x\Theta_{zz} + 2u_z\Theta_{xz}) \\ n(\mu u_x + \Psi_{xd}) \\ n(\mu u_x^2 + 2u_x\Psi_{xd} + \mu\Theta_{xx}) \\ n(\mu u_x u_y + u_x\Psi_{yd} + u_y\Psi_{xd} + \mu\Theta_{xy}) \\ n(\mu u_x u_z + u_x\Psi_{zd} + u_z\Psi_{xd} + \mu\Theta_{xz}) \\ n(\mu^2 u_x + 2\mu\Psi_{xd} + u_x\Psi_{dd}) \end{bmatrix}. \tag{4.15}$$

Again the flux in the y and z direction are symmetrical to $\boldsymbol{F}_x$. The source vector for Stokes flow, $\boldsymbol{S}$, is now

$$\boldsymbol{S} = \frac{n}{\tau_{\mathcal{G}}} \begin{bmatrix} 0 \\ V_x - (u_x - 2\Psi_{xd}) \\ V_y - (u_y - 2\Psi_{yd}) \\ V_z - (u_z - 2\Psi_{zd}) \\ 2\left(V_x(u_x - 2\Psi_{xd}) - (u_x^2 - 4u_x\Psi_{xd} + 4\Psi_{xd}^2 + \Theta_{xx})\right) \\ V_x(u_y - 2\Psi_{yd}) + V_y(u_x - 2\Psi_{xd}) - 2(u_xu_y - 2u_x\Psi_{yd} - 2u_y\Psi_{xd} + 4\Psi_{xd}\Psi_{yd} + \Theta_{xy}) \\ V_x(u_z - 2\Psi_{zd}) + V_z(u_x - 2\Psi_{xd}) - 2(u_xu_z - 2u_x\Psi_{zd} - 2u_z\Psi_{xd} + 4\Psi_{xd}\Psi_{zd} + \Theta_{xz}) \\ 2\left(V_y(u_y - 2\Psi_{yd}) - (u_y^2 - 4u_y\Psi_{yd} + 4\Psi_{yd}^2 + \Theta_{yy})\right) \\ V_y(u_z - 2\Psi_{zd}) + V_z(u_y - 2\Psi_{yd}) - 2(u_yu_z - 2u_y\Psi_{zd} - 2u_z\Psi_{yd} + 4\Psi_{yd}\Psi_{zd} + \Theta_{yz}) \\ 2\left(V_z(u_z - 2\Psi_{zd}) - (u_z^2 - 4u_z\Psi_{zd} + 4\Psi_{zd}^2 + \Theta_{zz})\right) \\ 0 \\ V_x(\mu - 2\Psi_{dd}) - (\mu u_x - 2\mu\Psi_{xd} - 2u_x\Psi_{dd} + 4\Psi_{dd}\Psi_{xd} + \Psi_{xd}) \\ V_y(\mu - 2\Psi_{dd}) - (\mu u_y - 2\mu\Psi_{yd} - 2u_y\Psi_{dd} + 4\Psi_{dd}\Psi_{yd} + \Psi_{yd}) \\ V_z(\mu - 2\Psi_{dd}) - (\mu u_z - 2\mu\Psi_{zd} - 2u_x\Psi_{dd} + 4\Psi_{dd}\Psi_{zd} + \Psi_{zd}) \\ 0 \end{bmatrix}, \tag{4.16}$$

where

$$\tau_{\mathcal{G}} = \frac{\rho_p}{18\mu_f} e^{2\mu - 2\Psi_{dd}} \tag{4.17}$$

The eigenvalues for this model take a clean, symmetric form as

$$\lambda_{1-15} = \begin{pmatrix} u_x + \sqrt{3\Theta_{xx}} \\ u_x - \sqrt{3\Theta_{xx}} \\ u_x + \sqrt{\Theta_{xx}} \\ u_x - \sqrt{\Theta_{xx}} \\ u_x + \sqrt{\Theta_{xx}} \\ u_x - \sqrt{\Theta_{xx}} \\ u_x + \sqrt{\Theta_{xx}} \\ u_x - \sqrt{\Theta_{xx}} \\ u_x \\ u_x \\ u_x \\ u_x \\ u_x \\ u_x \\ u_x \end{pmatrix}. \tag{4.18}$$

These represent the wave speeds defining information propagation in the PDEs. Ten of the eigenvalues are identical to the base ten-moment model, while five new eigenvalues that correspond to particle-size information propagation have appeared.

Numerical and analytical results from the model based on the average particle diameters were poorer as compared to the model based on the average logarithm of particle diameters. Only the second model, based on the average logarithm of the particle diameter, will be further analyzed in this work.

4.2 Proof of Well-posedness

Further analysis on the new higher-order moment models for multiphase flows with varying particle sizes is done in this section. An important property of the ten-moment equations is that, if the variance-covariance matrix Θ_{ij} is initially symmetric positive definite, it can be proven to remain this way [26]. The positive definiteness of Θ_{ij} for the traditional Gaussian model ensures that wavespeeds remain real and the distribution function remains properly defined. To show that the evolution of the new augmented variance-covariance matrix, Ψ, retains the same properties, the equations are first re-written in primitive form

$$\frac{\partial n}{\partial t} + u_k \frac{\partial n}{\partial x_k} + n \frac{\partial u_k}{\partial x_k} = 0\,, \tag{4.19}$$

$$\frac{\partial u_i}{\partial t} + u_k \frac{\partial u_i}{\partial x_k} + \frac{\Theta_{ik}}{n} \frac{\partial n}{\partial x_k} + \frac{\partial \Theta_{ik}}{\partial x_k} = \frac{1}{n} S_i\,, \tag{4.20}$$

$$\frac{\partial \Theta_{ij}}{\partial t} + u_k \frac{\partial \Theta_{ij}}{\partial x_k} + \Theta_{jk} \frac{\partial u_i}{\partial x_k} + \Theta_{ik} \frac{\partial u_j}{\partial x_k} = \frac{1}{n} \left(S_{ij} - u_j S_i - u_i S_j \right)\,, \tag{4.21}$$

$$\frac{\partial \mu}{\partial t} + u_k \frac{\partial \mu}{\partial x_k} + \frac{\Psi_{kd}}{n} \frac{\partial n}{\partial x_k} + \frac{\partial \Psi_{kd}}{\partial x_k} = 0\,, \tag{4.22}$$

$$\frac{\partial \Psi_{id}}{\partial t} + u_k \frac{\partial \Psi_{id}}{\partial x_k} + \Psi_{kd} \frac{\partial u_i}{\partial x_k} + \Theta_{ik} \frac{\partial \mu}{\partial x_k} = \frac{1}{n} \left(S_{di} - \mu S_i \right)\,, \tag{4.23}$$

$$\frac{\partial \Psi_{dd}}{\partial t} + u_k \frac{\partial \Psi_{dd}}{\partial x_k} + 2\Psi_{kd} \frac{\partial \mu}{\partial x_k} = 0\,. \tag{4.24}$$

Here, S_i represents the source term related to the equation produced with a generating weight of v_i, S_{ij} is the source term for the equation using the generating weight of $v_i v_j$ and S_{di} is the source term related to the generating weight $v_i ln(d)$. Here the

right-hand side Eqs. (4.20),(4.21) and (4.23) simplify to

$$RHS(4.20) = \frac{1}{\tau}\left(V_i - (u_i - 2\Psi_{id})\right) , \tag{4.25}$$

$$RHS(4.21) = \frac{1}{\tau}\left(-2V_i\Psi_{jd} - 2V_j\Psi_{id} + u_i\Psi_{jd} + 2u_j\Psi_{id} + 4\Psi_{id}\Psi_{jd} + 2\Theta_{ij}\right) , \tag{4.26}$$

$$RHS(4.23) = \frac{1}{\tau}\left(-2V_i\Psi_{dd} + 2u_i - 4\Psi_{id}\Psi_{dd} - \Psi_{id}\right) . \tag{4.27}$$

To prove that the variance-covariance matrix, Ψ, remains symmetric positive definite, one needs to multiply the inverse of Ψ to the evolution equation for Ψ and then take the trace of it. By using a block matrix technique, this expands to

$$\mathrm{tr}\left(\begin{bmatrix} A_{ij} & B_i \\ B_j & C \end{bmatrix}\begin{bmatrix} LHS(4.21) & LHS(4.23) \\ LHS(4.23) & LHS(4.24) \end{bmatrix}\right) = \mathrm{tr}\left(\begin{bmatrix} A_{ij} & B_i \\ B_j & C \end{bmatrix}\begin{bmatrix} RHS(4.21) & RHS(4.23) \\ RHS(4.23) & RHS(4.24) \end{bmatrix}\right) . \tag{4.28}$$

Here, $LHS()$, is the left hand side of the respective equation, A_{ij}, B_i, B_j and C are the block matrices of the inverse of Ψ and have the form

$$\begin{aligned} A_{ij} &= (\Theta_{ij} - \Psi_{id}\Psi_{jd}\Psi_{dd}^{-1})^{-1} , \\ B_i &= -A_{ij}\Psi_{jd}\Psi_{dd}^{-1} , \\ B_j &= B_i^T , \\ C &= \Psi_{dd}^{-1} + \Psi_{dd}^{-2}(A_{ij}\Psi_{id}\Psi_{jd}) . \end{aligned}$$

Eq. (4.28) expands to

$$\begin{aligned} &\mathrm{tr}\left(A_{ij}LHS(4.21) + 2B_iLHS(4.23)\right) + C\ LHS(4.24) \\ =&\mathrm{tr}\left(A_{ij}RHS(4.21) + 2B_iRHS(4.23)\right) + C\ RHS(4.24) . \end{aligned} \tag{4.29}$$

Replacing the B_i, C_i in the equation simplifies to

$$\begin{aligned} &\mathrm{tr}\Big(A_{ij}\left(\frac{D}{Dt}\Theta_{ij} + \frac{2}{\Psi_{dd}}\Psi_{id}\frac{D}{Dt}\Psi_{jd} + \frac{1}{\Psi_{dd}^2}\Psi_{id}\Psi_{jd}\frac{D}{Dt}\Psi_{dd}\right) + \\ &\qquad \frac{1}{\Psi_{dd}}\frac{D}{Dt}\Psi_{dd} + 2A_{ij}\underbrace{\left(\Theta_{ik} - \frac{1}{\Psi_{dd}}\Psi_{id}\Psi_{kd}\right)}_{A_{ij}^{-1}}\frac{\partial u_j}{\partial x_k} + \\ &\underbrace{A_{ij}\left(\frac{-2}{\Psi_{dd}}\Psi_{id}\Theta_{jk} + \frac{2}{\Psi_{dd}^2}\Psi_{id}\Psi_{jd}\Psi_{kd}\right)\frac{\partial \mu}{\partial x_k} + \frac{2}{\Psi_{dd}}\Psi_{kd}\frac{\partial \mu}{\partial x_k}}_{=0}\Big) = -\frac{6}{\tau} . \end{aligned} \tag{4.30}$$

Note that $\frac{D}{Dt}$ is the calculation of the material derivative shown as

$$\frac{D()}{Dt} = \frac{\partial()}{\partial t} + u_i \frac{\partial()}{\partial x_i} \,. \tag{4.31}$$

Then, the identity $\partial_s \log(\det(\Psi)) = tr(\Psi^{-1}\partial_s \Psi)$ is used with Eq. (4.19) to reduce the equation to

$$\frac{D}{Dt}\log(\det \Psi) - \frac{2}{\mathrm{n}}\frac{D}{Dt}\log\left(\frac{1}{\mathrm{n}^2}\right) + 2\frac{\partial u_k}{\partial x_k} - 2\frac{\partial u_k}{\partial x_k} = -\frac{6}{\tau} \,. \tag{4.32}$$

Finally, this can be simplified to a simple convection equation

$$\frac{DY}{Dt} = -\frac{6}{\tau} \,, \tag{4.33}$$

where Y is expressed as $Y = \log\left(\frac{\det \Psi}{n^2}\right)$. Since the value of n is always positive, it is clear from Eq. (4.33) that, for any initial condition of the augmented variance-covariance matrix Ψ that respects the realizable limits, the matrix will remain symmetric positive definite. This is enough to guarantee that the distribution function remains properly integrable. It also guarantees that the wavespeeds in the system remain real valued, which proves the model remains hyperbolic.

4.3 Moment Model in Spherical Coordinate System

In some situations, it is more efficient to solve the problem using a spherical coordinate system. Contrary to numerical solutions using a Cartesian coordinate system, where the cells in the mesh are of equal volume, the cell volumes in a spherical coordinate system increase with distance from the origin. This increase in volume can be represented as a geometric source term in 1D spherical symmetry. The spherical coordinate source term can be derived by taking the divergence of the flux term in spherical coordinates. Using the assumption of spherical symmetry, the equations can be simplified to

$$\frac{\partial \boldsymbol{U}}{\partial t} + \frac{\partial \boldsymbol{F}_r}{\partial r} = \boldsymbol{S_{sc}} \,. \tag{4.34}$$

A spherical geometry source term, $\boldsymbol{S_{sc}}$, result from the change of coordinate system and takes into account the increase in volume in each cell. It has the form

$$\boldsymbol{S_{sc}} = \begin{bmatrix} -\frac{2}{r} n u_x \\ -\frac{1}{r}\left(2n(u_x^2 + \Theta_{xx}) - n\Theta_{yy} - n\Theta_{zz}\right) \\ -\frac{2}{r}\left(n(u_x^3 + 3u_x\Theta_{xx} - u_x\Theta_{yy} - u_x\Theta_{zz})\right) \\ -\frac{4}{r} n u_x \Theta_{yy} \\ -\frac{4}{r} n u_x \Theta_{zz} \\ -\frac{2}{r}\left(n(\mu u_x + \Psi_{xd})\right) \\ -\frac{1}{r}\left(2n(\mu u_x^2 + 2u_x\Psi_{xd} + \mu\Theta_{xx}) - n\mu\Theta_{yy} - n\mu\Theta_{zz}\right) \\ -\frac{2}{r} n\left(\mu^2 u_x + 2\mu\Psi_{xd} + u_x\Psi_{dd}\right) \end{bmatrix}. \tag{4.35}$$

This spherical coordinate system is divided by the radius, creating a singularity near zero. If this becomes a problem during numerical solutions, it is possible to multiply the equation by r^2. The new evolution becomes

$$r^2\frac{\partial \boldsymbol{U}}{\partial t} + r^2\frac{\partial \boldsymbol{F}_r}{\partial r} = r^2\boldsymbol{S_{sc}}\,, \tag{4.36}$$

$$\frac{\partial \widetilde{\boldsymbol{U}}}{\partial t} + \frac{\partial \widetilde{\boldsymbol{F}}_{\boldsymbol{r}}}{\partial r} = \widetilde{\boldsymbol{S}}_{\boldsymbol{sc}}\,. \tag{4.37}$$

The resulting spherical source term for the new conserved solution vector is

$$\widetilde{\boldsymbol{S}}_{\boldsymbol{sc}} = \begin{bmatrix} 0 \\ rn\left(\Theta_{\theta\theta} + \Theta_{\psi\psi}\right) \\ 2rnu_r\left(\Theta_{\theta\theta} + \Theta_{\psi\psi}\right) \\ -2rnu_r\Theta_{\theta\theta} \\ -2rnu_r\Theta_{\psi\psi} \\ 0 \\ rn\mu\left(\Theta_{\theta\theta} + \Theta_{\psi\psi}\right) \\ 0 \end{bmatrix}. \tag{4.38}$$

Solving for this new solution vector, $\widetilde{\boldsymbol{U}}$, has the advantages of eliminating the risk of creating a singularity near zero. It is also possible to calculate the previous form of the variables easily from the solution.

4.4 Reduction of the Polydisperse Moment Model to One Dimension

This initial study of the proposed Polydisperse Gaussian is restricted to one-dimensional problems. The one-dimensional models results from assuming that no property varies in the y or z directions. The generating weight, $\boldsymbol{W}$, the solution vector, $\boldsymbol{U}$, and flux

vector, $\boldsymbol{F}_x$, takes the form

$$\boldsymbol{W} = \begin{bmatrix} 1 \\ v_x \\ v_x^2 \\ v_y^2 \\ v_z^2 \\ \ln d \\ v_x \ln d \\ \ln(d)^2 \end{bmatrix} \quad \boldsymbol{U} = \begin{bmatrix} n \\ nu_x \\ n(u_x^2 + \Theta_{xx}) \\ n\Theta_{yy} \\ n\Theta_{zz} \\ n\mu \\ n(\mu u_x + \Psi_{xd}) \\ n(\mu^2 + \Psi_{dd}) \end{bmatrix} \quad \boldsymbol{F}_x = \begin{bmatrix} nu_x \\ n(u_x^2 + \Theta_{xx}) \\ n(u_x^3 + 3u_x\Theta_{xx}) \\ nu_x\Theta_{yy} \\ nu_x\Theta_{zz}) \\ n(\mu u_x + \Psi_{xd}) \\ n(\mu u_x^2 + 2u_x\Psi_{xd} + \mu\Theta_{xx}) \\ n(\mu^2 u_x + 2\mu\Psi_{xd} + u_x\Psi_{dd}) \end{bmatrix}. \tag{4.39}$$

The 1D source vector is reduces to

$$\boldsymbol{S} = \frac{n}{\tau_{\mathcal{G}}} \begin{bmatrix} 0 \\ V_x - (u_x - 2\Psi_{xd}) \\ 2\left(V_x(u_x - 2\Psi_{xd}) - (u_x^2 - 4u_x\Psi_{xd} + 4\Psi_{xd}^2 + \Theta_{xx})\right) \\ 2\Theta_{yy} \\ 2\Theta_{zz} \\ 0 \\ V_x(\mu - 2\Psi_{dd}) - (\mu u_x - 2\mu\Psi_{xd} - 2u_x\Psi_{dd} + 4\Psi_{dd}\Psi_{xd} + \Psi_{xd}) \\ 0 \end{bmatrix}. \tag{4.40}$$

4.5 Analytical Solution of the Full Kinetic Equation

For initial-value problems on an infinite domain for still background flow the exact solution to the full kinetic equation, Eq. (3.7), has been constructed. For flows of particles with a range of diameters, described by Eq. (3.7), on an infinite domain with initial particle distribution given by

$$\mathcal{F}_0(x_i, v_i, d)\,, \tag{4.41}$$

the exact solution at any future time is given by

$$\mathcal{F}(x_i, v_i, d, t) = A\,\mathcal{F}_0(B_i, C_i, d)\,, \tag{4.42}$$

with $A = e^{\frac{3t}{\tau}}$, $B_i = x_i + v_i\tau(1 - e^{\frac{t}{\tau}})$ and $C_i = v_i e^{\frac{t}{\tau}}$. The derivation of this exact solution can be found in Appendix A. The availability of this exact solution allows one to directly study any errors that arise from the modelling assumptions that have been made.

Chapter 5

Application to Monodisperse Flows

5.1 An Illustrative Problem Involving Crossing Beams

As one of the interest of this work is the investigation of the capability for moment closures to accurately predict monodisperse particle-stream crossing, an illustrative flow problem is adopted. This two-dimensional problem was originally used by Vié *et al.* [51]. It consist of two stream of particles moving through a fixed, compressible background flow. This background flow has a imposed velocity field given by

$$V_x = 0.2\,\mathrm{m/s}$$
$$V_y = -\varepsilon y\,.$$

For the present study, ε is taken to be $1.0\,\mathrm{s}^{-1}$. Essentially, the background flow velocity is constant in the x-direction and provides a compressive acceleration field in the y-direction.

The domain of interest is chosen to be $0\,\mathrm{m} < x < 5\,\mathrm{m}$ and $-1\,\mathrm{m} < y < 1\,\mathrm{m}$. Along the edge with $x = 0\,\mathrm{m}$, two beams of particles enter. The first beam spans $-0.6\,\mathrm{m} < y < -0.4\,\mathrm{m}$ while the second spans $0.4\,\mathrm{m} < y < 0.6\,\mathrm{m}$. Each beam has an initial density of $\rho = 1.0\,\mathrm{kg/m}^3$, $u_x = 0.2\,\mathrm{m/s}$ and $u_y = 0.0\,\mathrm{m/s}$.

As the particles have the same speed in the x direction as the background flow, they experience no x-direction acceleration. The y-direction motion of a particle is described by the ordinary differential equations

$$\frac{\partial Y_p}{\partial t} = u_p\,, \quad \frac{\partial u_p}{\partial t} = -\frac{1}{\tau_p}\left(u_p - V_y(Y_p)\right) = -\frac{1}{\tau_p}\left(u_p + \varepsilon Y_p\right)\,. \tag{5.1}$$

Here, Y_p and u_p are the Lagrangian position and velocity of a particle. The particle relaxation time, τ_p, is fixed to 5.0 s. Combining these equations results in a scalar second-order equation that describes the vertical motion of the particles,

$$\frac{\partial^2 Y_p}{\partial t} + \frac{\partial Y_p}{\partial t} + \frac{\varepsilon}{\tau_p} Y_p = 0\,. \tag{5.2}$$

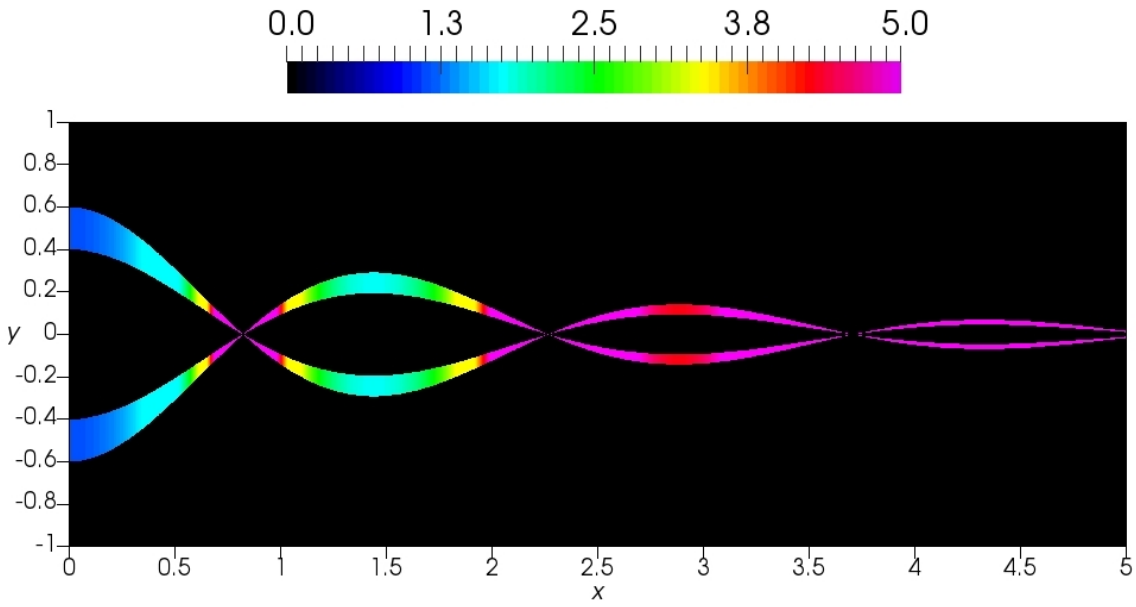

Figure 5.1: Exact solution of the particle density of two crossing beams of non-interacting particles in a fixed compressive background velocity field.

This equation can be used to build an exact solution for this problem. Following Vié *et al.*, if one defines a Stokes number, $\mathrm{St} = \varepsilon\tau_p$, $\omega^2 = \frac{1}{4}\left|\frac{1}{\tau_p^2} - \frac{4\varepsilon}{\tau_p}\right|$, and a critical Stokes number as $\mathrm{St}_c = \frac{1}{4}$. The solution can be expressed as

$$Y_p(t) = Y_{p0}\exp\left(-\frac{t}{2\tau_p}\right)\begin{cases}\exp(-\omega t) & \text{if } \mathrm{St} \leq \mathrm{St}_c\,,\\ \cos(-\omega t) - \frac{1}{2\omega\tau_p}\sin(-\omega t) & \text{otherwise}\,.\end{cases} \tag{5.3}$$

The x position of a particle, X_p, is simply given by

$$X_p(t) = V_x t = (0.2\,\mathrm{m/s})t. \tag{5.4}$$

Eqs. (5.3) and (5.4) can be used to determine the trajectories of the particles at the edge of each beam. The density of each beam at a particular x coordinate is inversely proportional to the width of the beam. The exact solution for this problem is shown in Figure 5.1. It can clearly be seen that the two distinct beams cross three times within the domain. Such solutions have traditionally been very difficult to obtain with Eulerian methods. As an added complication, the density field is singular at the three crossing locations [9].

5.1.1 Reduction of the Moment Model to One Dimension

From a Lagrangian perspective, the two-dimensional problem presented in Section 6.1 is actually a one-dimensional problem in a moving frame of reference that moves in the x direction along with both the particle phase and background flow with a velocity of $V_x = 0.2\,\mathrm{m/s}$. In this frame of reference, the x component of the velocity of each particle remains zero in the exact solution.

The kinetic description of the particle phase can also be reduced to a one-dimensional treatment. This is done by assuming that both the position, y, and y-direction velocity, v, of each particle are scalars. The kinetic equation describing the evolution of the distribution function, $\mathcal{F}(y, v, t)$, becomes

$$\frac{\partial \mathcal{F}}{\partial t} + v\frac{\partial \mathcal{F}}{\partial y} + \frac{\partial}{\partial v}\left(a\mathcal{F}\right) = 0\,, \tag{5.5}$$

where a is the scalar acceleration in the y direction. Moments of the one-dimensional distribution are now defined as

$$\begin{aligned} \rho &= \langle m\mathcal{F}\rangle\,, & \rho u &= \langle mv\mathcal{F}\rangle\,, & p &= \left\langle mc^2\mathcal{F}\right\rangle\,, \\ q &= \left\langle mc^3\mathcal{F}\right\rangle\,, & r &= \left\langle mc^4\mathcal{F}\right\rangle\,, & s &= \left\langle mc^5\mathcal{F}\right\rangle\,. \end{aligned} \tag{5.6}$$

All moments are now scalars.

Of the four moment methods shown in Section 3.4.1, three can naturally preserve the one-dimensional nature of such flows. The five-moment Euler model shown in Eqs. (3.28)–(3.30) cannot naturally maintain the one-dimensional nature of a particle flow. This is because the model assumes a variance-covariance matrix of particle velocities given by $\Theta_{ij} = \theta\delta_{ij}$. That is, particle velocities are forced to have the same variance in all directions. If the particle velocities have a variance in one direction, as they do in the y direction at the crossing point of the streams in the problem described above, this variance is automatically distributed in all directions by the model and the one-dimensional character of the situation is lost. For the remaining methods, a one-dimensional solver is used for this problem. This is done so that very high resolutions can be affordably used. The goal is to be able to solve the problem using the three models with a high enough accuracy that numerical errors

are insignificant and the true predictive capabilities of the models themselves can be assessed. As the five-moment Euler system cannot be solved in one dimension, the example solution for it is computed using a reduced resolution and a two-dimensional solver. As the ten-moment model and fourteen-moment model allows for different particle-velocity variances in different directions, they do not suffer from this limitation of the five-moment Euler description. In the study of the multiphase problem described above, solutions for the single-velocity, ten-moment, and fourteen-moment models are obtained by solving the one-dimensional form of the equations shown in Section 3.5.

5.2 Numerical Method

The numerical method in this research uses a higher-order Godunov-type finite-volume method to compute the various solutions [13]. In a finite-volume scheme, the domain of interest is divided into equal sized cells. The scheme uses a piecewise limited-linear reconstruction in space and a predictor-corrector time marching technique. The limiter used in all cases is the minmod limiter [38]. For very low Stokes numbers, the source term can become excessively stiff. Due to the linear nature of this local term, a point-implicit time-marching method can be easily adopted that treats the hyperbolic flux term explicitly, while using an implicit treatment for the source term. The predictor step to update the average solution state in cell i can be expressed as

$$\begin{aligned}\hat{\bar{\boldsymbol{U}}}_i &= \bar{\boldsymbol{U}}_i^n + \Delta t \left[\frac{-1}{\Delta y}(F_{i+\frac{1}{2}} - F_{i-\frac{1}{2}}) + S_i^{n+1}\right] \\ &= \bar{\boldsymbol{U}}_i^n + \Delta t \left[\frac{-1}{\Delta y}(F_{i+\frac{1}{2}} - F_{i-\frac{1}{2}}) + S_i^n + \frac{\mathrm{d}S}{\mathrm{d}U}\left(U_i^{n+1} - U_i^n\right)\right] . \end{aligned} \tag{5.7}$$

Here $\bar{\boldsymbol{U}}_i$ is the average value of the conserved solution vector in cell i, $F_{i-\frac{1}{2}}$ is the flux between cells $i-1$ and i, while $F_{i+\frac{1}{2}}$ is the flux between cell i and $i+1$, S_i is the source vector evaluated at the centroid and Δt is the time step interval. This can be rearranged to give

$$\hat{\bar{\boldsymbol{U}}}_i = \bar{\boldsymbol{U}}_i^n + \Delta t \left[I - \Delta t \frac{\mathrm{d}S}{\mathrm{d}U}\right]^{-1} \left(\frac{-1}{\Delta y}(F_{i+\frac{1}{2}} - F_{i-\frac{1}{2}}) + S_i^n\right) , \tag{5.8}$$

Then the corrector step can be expressed as

$$\bar{\boldsymbol{U}}_i^{n+1} = \bar{\boldsymbol{U}}_i^n + \Delta t \left[I - \frac{\Delta t}{2} \frac{\mathrm{d}S}{\mathrm{d}U} \right]^{-1} \quad \left(\frac{-1}{2\Delta y} (F_{i+\frac{1}{2}} + \hat{F}_{i+\frac{1}{2}} - F_{i-\frac{1}{2}} - \hat{F}_{i-\frac{1}{2}}) + S_i^n \right). \tag{5.9}$$

Where $\hat{F}$ is the flux calculated at the predictor state. The numerical fluxes between each cell are calculated using the HLL flux function [18]. For all but the fourteen-moment model, the wavespeeds of the systems are known analytically. However, for the fourteen-moment system, closed-form expressions for the wavespeeds are not available. Instead, when a wavespeeds is needed, the flux Jacobian is formed analytically and its eigenvalues are numerically computed. The source vector for Stokes flow is linear with respect to the moments in the solution vector. Its Jacobian is therefore constant throughout a calculation.

5.3 Numerical Results

In the exact solution of the problem described above, the majority of the domain contains no particles. This is problematic for the Eulerian models used in this work, as division-by-zero errors will occur. In order to avoid such problems, a uniform background density of particles with $\rho = 10^{-6}\,\mathrm{kg/m^3}$ is assumed. For models that contain the moment p, an initial value of $p = 10^{-11}\,\mathrm{Pa}$ is chosen. If, during a calculation, numerical errors cause the average pressure or density in one cell to dip below zero, it is reset to its initial small value. For the fourteen-moment model, there is another singularity present when $\sigma \to 0$. In order to avoid numerical difficulties, σ is restricted to remain in the domain $2 \times 10^{-4} \leq \sigma \leq 1$. If σ slightly leaves this domain during calculation, it is reset to the appropriate limit of the allowable values. The initial condition for σ is 2×10^{-4} everywhere.

For the models that can be solved using a one dimensional solver, the initial conditions are that $u = 0$ everywhere. For $-0.6\,\mathrm{m} < y < -0.4\,\mathrm{m}$, the density is set to the density of the bottom beam. For $0.4\,\mathrm{m} < y < 0.6\,\mathrm{m}$, the density is that of the top beam. Within each beam, $p = 10^{-5}\,\mathrm{Pa}$ for the models with this variable. The domain is $-1\,\mathrm{m} < y < 1\,\mathrm{m}$ with the top and bottom boundary conditions held at the

initial background values. For all cases, to ensure numerical error remain negligible, a grid of 10,000 equally sized cells is used. A CFL number of 0.5 is chosen.

The Euler model cannot be solved in one dimension. A two-dimensional solver is therefore used. In this case, the domain is $0\,\mathrm{m} < x < 5\,\mathrm{m}$ and $-1\,\mathrm{m} < y < 1\,\mathrm{m}$. The domain is divided into 2,500 cell in the x direction and 1,000 cells in the y direction. Boundary conditions are held fixed at the background values everywhere, except on the left side where the particle streams enter. At these two locations, the state is held fixed at the values describing the beams. Again, a CFL number of 0.5 is used.

5.3.1 Symmetric Crossing Beams

Numerical solutions for the case of two symmetric beams are shown in Figure 5.2. As expected, the single-velocity solution, shown in Figure 5.2(a), is woefully inadequate. The assumption that all particles at a point share the same velocity does not allow any form of particle-stream crossing. The two beams simply compress into a single, extremely dense beam that exits to the right.

Figure 5.2(b) shows the Euler solutions. One can see that, at the first crossing point, particles can take on a range of velocities. However, as the model forces the variance to be isotropic, particles spray out in all directions. The solution after this does not well approximate the true solution and contains spurious, discontinuous shock waves.

From the ten-moment model, solutions begins to improve drastically. In Figure 5.2(c), the particle streams do not cross cleanly, however, the solution does seem to follow the general shape of the exact solution. This is the same finding that was observed by Vié *et al.* [51].

By moving from the ten-moment model to the fourteen-moment model, Figure 5.2(d), one again observes a marked improvement in the solution. The model's underlying bi-modal distribution function allows the particles in the crossing jets to cleanly take on two distinct velocities. In the solution, the stream's criss-cross pattern agrees extremely well with the exact solution. Clearly, in the maximum-entropy hierarchy of closures, the fourteen-moment closure is the lowest-order model that

correctly allows particle-stream crossing. It is important to note that it would be possible to solve this problem with a lower-order member model using two families of particles but in practical application it is unknown if particles crossing will occurs. Therefore, it is difficult to decide beforehand if using two families of particles useful.

5.3.2 Crossing Beams of Different Densities

Investigation of the 10-moment prediction for symmetric particle beams does not make it clear if one can say that the particle beams are crossing or not. This question can easily be settled by varying the particle density in one of the beams. Figure 5.3 shows the same case of crossing jets, but with the top jet having double the original density. In the exact solution, at each crossing, the denser beam crosses and alternates between being above and bellow the less dense beam. The single-velocity model again predicts the particle beams collapsing into one stream that exits to the right. The ten-moment solution does not seem to allow crossing either. Rather, the two beams seem to reflect off each other. Also, the solution no longer seems to stay within the y-coordinate limits of the exact solution. The bottom stream reflects far further than the limit of the exact solution, while the top stream reflects far less.

The fourteen-moment solution for this case remains very close to the exact solution. It is clear that the streams are genuinely crossing, as the denser stream correctly alternates between being above and below the less dense stream—exactly as happens in the exact solution. Again, the agreement between the exact solution and the prediction by the fourteen-moment model is extremely high.

In Figures 5.4 and 5.5, the density ratio is increased to 4 and then 8. In both cases, the previous behaviours continue. Notably, the single stream of particles predicted by the single-velocity model after the first crossing points now follows an oscillatory path through the domain. The asymmetry of the trajectories predicted by the ten-moment models become more extreme, always bouncing off each other, rather than crossing. In both cases, the fourteen-moment solutions are in very good agreement with the exact solution. This higher-order model predicts clean crossing of the streams, and the trajectories are not altered by the differing densities.

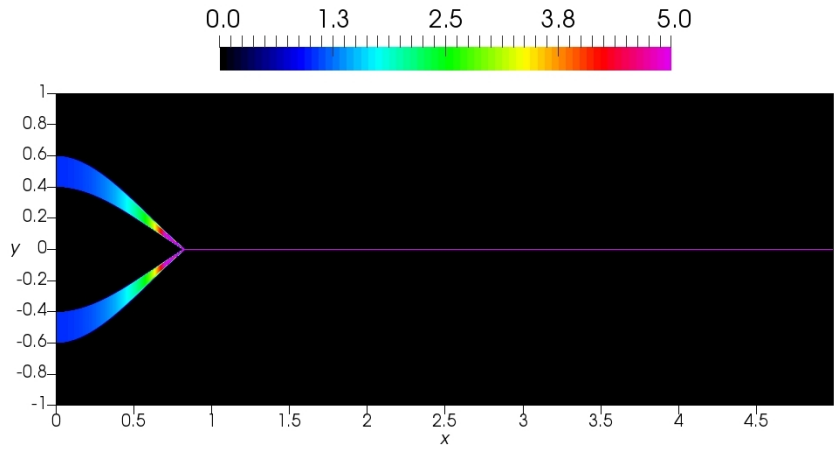

(a) Single-velocity prediction

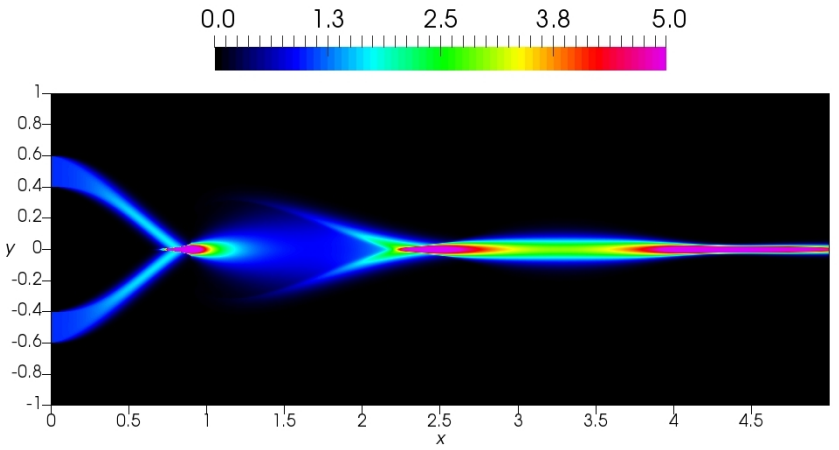

(b) Euler prediction

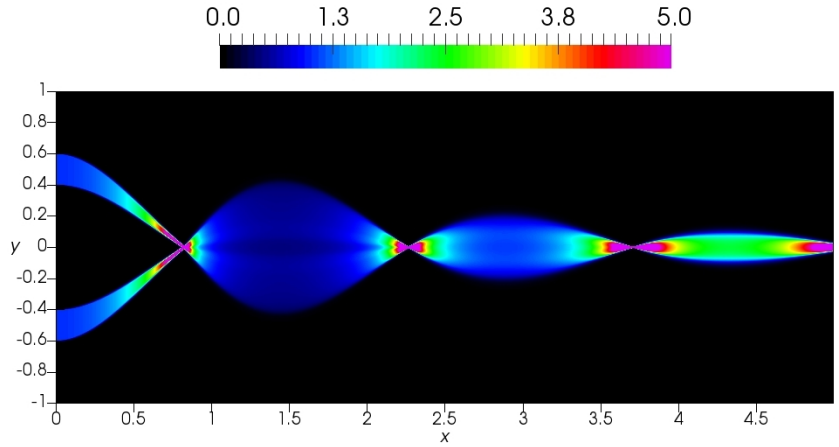

(c) Ten-moment prediction

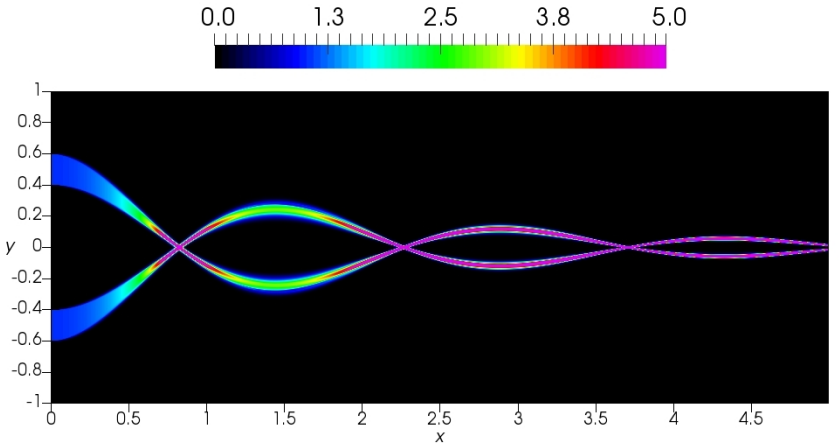

(d) Fourteen-moment prediction

Figure 5.2: Particle density of two crossing beams of non-interacting particles in a fixed compressive background velocity field.

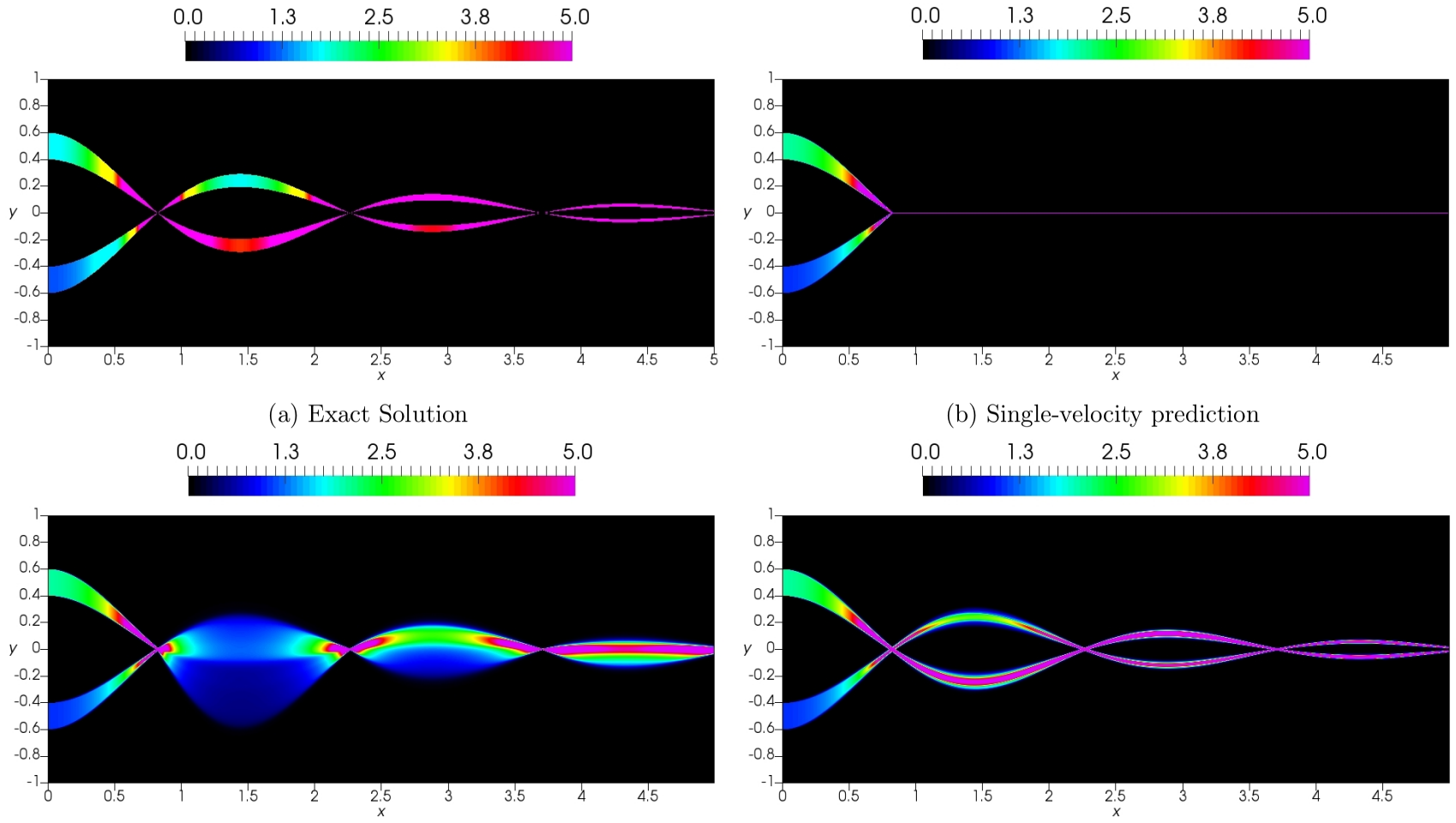

(a) Exact Solution

(b) Single-velocity prediction

(c) Ten-moment prediction

(d) Fourteen-moment prediction

Figure 5.3: Particle density of two crossing beams of non-interacting particles in a fixed compressive background velocity field, $\rho_{\text{top}} = 2\,\text{kg/m}^3$ and $\rho_{\text{bottom}} = 1\,\text{kg/m}^3$.

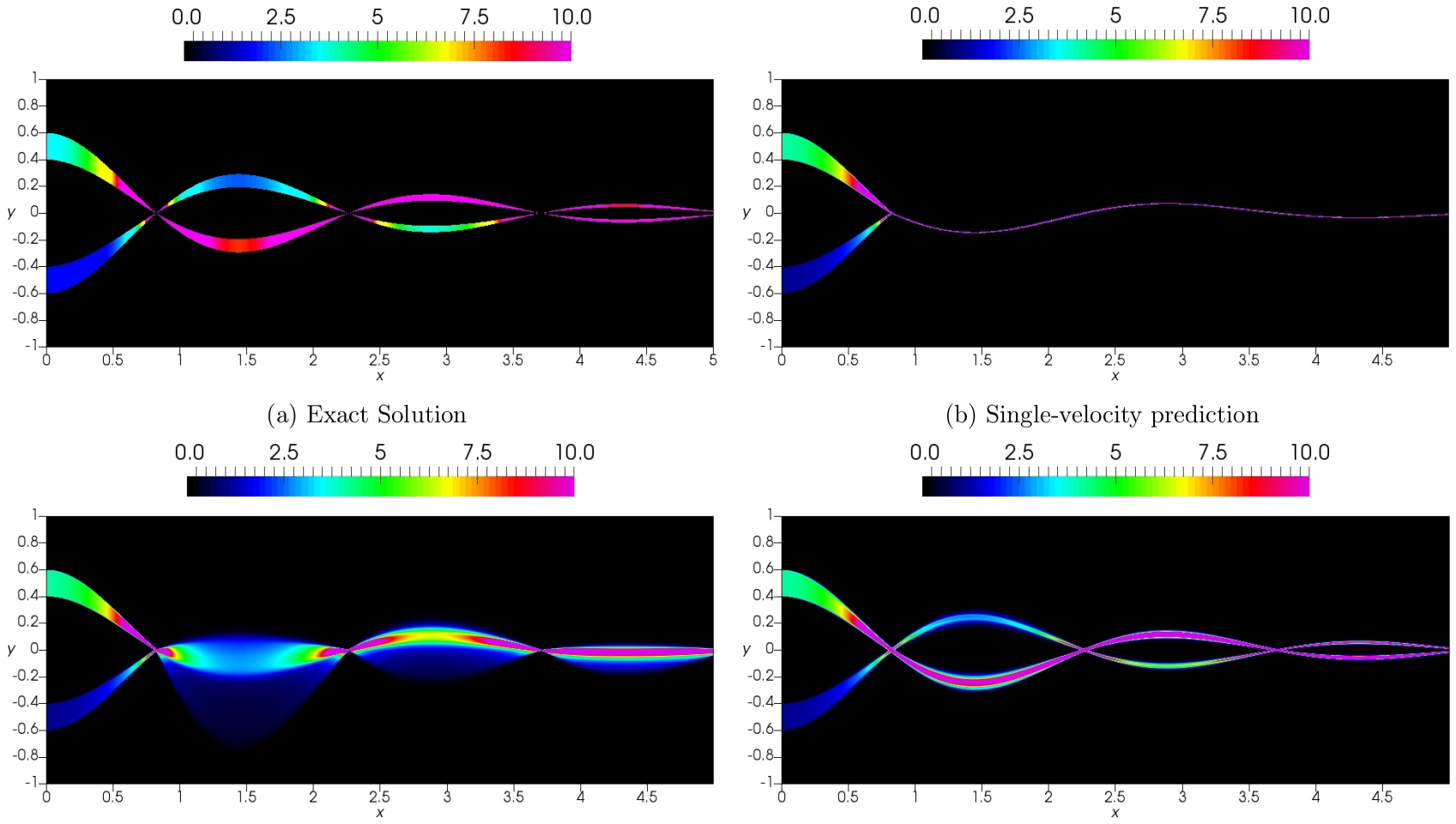

(a) Exact Solution

(b) Single-velocity prediction

(c) Ten-moment prediction

(d) Fourteen-moment prediction

Figure 5.4: Particle density of two crossing beams of non-interacting particles in a fixed compressive background velocity field, $\rho_{\text{top}} = 4\,\text{kg/m}^3$ and $\rho_{\text{bottom}} = 1\,\text{kg/m}^3$.

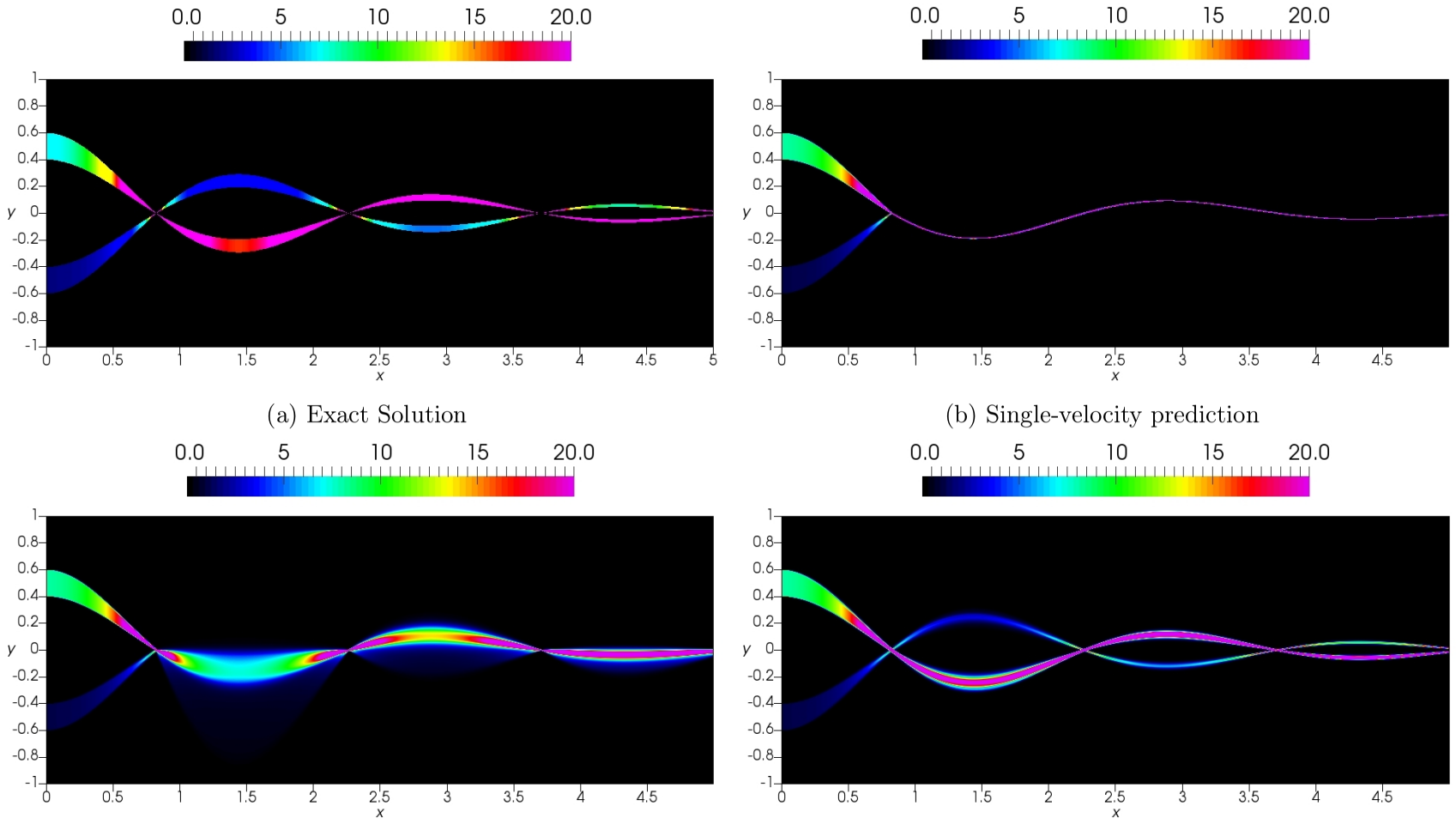

(a) Exact Solution

(b) Single-velocity prediction

(c) Ten-moment prediction

(d) Fourteen-moment prediction

Figure 5.5: Particle density of two crossing beams of non-interacting particles in a fixed compressive background velocity field, $\rho_{\text{top}} = 8\,\text{kg/m}^3$ and $\rho_{\text{bottom}} = 1\,\text{kg/m}^3$.

Chapter 6

Application to Polydisperse Flows

6.1 Simple Illustrative Problems

As a first study into the abilities of the closure to approximate solutions of the full, high-dimensional kinetic equation, two simple problems are considered. In both cases, the velocity of the background flow is assumed to be zero. This is chosen because the exact solution to the full kinetic equation, Eq. (3.7), has been constructed, for initial-value problems on an infinite domain for constant background flow, as shown in Section 4.5.

The first scenario considered is chosen to illustrate the effect of the drag in situation where the particles have a range of sizes and initial velocities. It consist of a simple space-homogeneous problem. The second scenario considered is a Riemann problem. A Riemann problem consists of a initial value problem containing a single discontinuity. Shock or rarefaction waves can appear as characteristics of the solution. It is possible to observe the different wavespeeds of a model. This second scenario is tested at different intensities of the source term to observe the effect of drag on the new model.

6.2 Numerical Method

The numerical method used is a simple first-order Godunov-type finite-volume method, with a slight variation. For this study, operator splitting is used. The hyperbolic part of the PDEs is treated explicitly, while the source term related to drag is evaluated analytically. The drag term in the polydisperse model is even more stiff than its monodisperse counterpart. Any numerical error can easily bring the model out of realizable state. Having operator splitting and treating the drag term analytically ensures the model's distribution function remains positive definite. In 1D, the first

step of the explicit scheme can be expressed as

$$\tilde{\boldsymbol{U}}_i^{\,s} = \bar{\boldsymbol{U}}_i^{s} - \frac{\Delta t}{\Delta x}\left(\hat{\boldsymbol{F}}_{i+\frac{1}{2}} - \hat{\boldsymbol{F}}_{i-\frac{1}{2}}\right), \tag{6.1}$$

where $\bar{\boldsymbol{U}}_i^{\,s}$ and $\tilde{\boldsymbol{U}}_i^{\,s}$ are the averagec onserved solution vectors in cell i at the beginning of the time step s and the intermediate step, before the contribution of the drag term is applied analytically, respectively. The inter-cellular numerical fluxes in Eq.(6.1), $\hat{\boldsymbol{F}}_{i\pm\frac{1}{2}}$, are calculated using the Harten-Lax-van Leer (HLL) flux function [18].

6.2.1 Analytical Source Term

Following the update of the intermediate solution vector $\tilde{\boldsymbol{U}}_i^{\,s}$, the contribution of the source term can be calculated analytically with the correposponding primitive variables $\tilde{\boldsymbol{W}}_i^{\,s}(\tilde{\boldsymbol{U}}_i^{\,s})$. The derivation of the analytic solution for the system of Eqs. (4.19)-(4.24) in a space-homogeneous case (*i.e.*, the spatial derivatives are equal to zero and only the source term is enabled) is presented here. One could easily make the following observations related to the source term:

- Eq. (4.19),(4.22) and 4.24 are time invariant,
- Eq. (4.20) and (4.23) are coupled only with one another, and
- Eq. (4.21) uses information from Eq. (4.20) and (4.23) in addition to the local variables.

The first observation implies the primitive variables n, μ and Ψ_{dd} remain constant in time. Based on the second observation, the solution u_x and Ψ_{xd} of Eq. (4.20) and (4.23) can be obtained by decoupling the system into laws of natural growth using an eigenvalue decomposition approach. Finally, the solution Θ_{xx} of Eq. (4.21) is obtained by using the expressions for u_x and Ψ_{xd} and followed by reduction to a set of decoupled laws of natural growth. These steps are presented in detail below.

The time-invariant solution for n, μ and Ψ_{dd} is

$$n(t) = n(0) \tag{6.2}$$

$$\mu(t) = \mu(0) \tag{6.3}$$

$$\Psi_{dd}(t) = \Psi_{dd}(0)\,. \tag{6.4}$$

Eqs. (4.20) and (4.23) in the space homogeneous can be written as

$$\frac{\mathrm{d}\hat{U}}{\mathrm{d}t} = \frac{1}{\tau_{\mathcal{G}}} A\hat{U} + C\,, \tag{6.5}$$

where $\hat{U} = [u_x\, \Psi_{xd}]^T$, A is a constant coefficient matrix

$$A = \begin{bmatrix} -1 & 2 \\ 2\Psi_{dd} & -(4\Psi_{dd}+1) \end{bmatrix}\,, \tag{6.6}$$

and C is related to the background flow velocity as

$$C = \frac{1}{\tau_{\mathcal{G}}} \begin{bmatrix} V_x \\ -2V_x\Psi_{dd} \end{bmatrix}\,. \tag{6.7}$$

Then, Eq. (6.5) is expressed using the eigenvalues decomposition $A = R\Lambda R^{-1}$ as

$$\frac{\mathrm{d}\hat{U}}{\mathrm{d}t} = \frac{1}{\tau_{\mathcal{G}}} R\Lambda R^{-1}\hat{U} + C\,, \tag{6.8}$$

and diagonalizing

$$\frac{\mathrm{d}R^{-1}\hat{U}}{\mathrm{d}t} = \frac{1}{\tau_{\mathcal{G}}} \Lambda R^{-1}\hat{U} + R^{-1}C\,, \tag{6.9}$$

where R and Λ is the eigenvector matrix, and the diagonal matrix of eigenvalues of A, respectively. Finally, two decoupled linear equations are obtained that can be solved analytically

$$\frac{\mathrm{d}}{\mathrm{d}t}\left[R^{-1}\hat{U}\right] = \frac{1}{\tau_{\mathcal{G}}} \begin{bmatrix} \hat{\lambda}_0 \\ \hat{\lambda}_1 \end{bmatrix} R^{-1}\hat{U} + \begin{bmatrix} C_0 \\ C_1 \end{bmatrix}\,. \tag{6.10}$$

The eigenvalues of A are

$$\hat{\lambda}_{0,1} = -\left(1 + 2\Psi_{dd} \pm 2\alpha\right)\,, \tag{6.11}$$

where

$$\alpha = \sqrt{\Psi_{dd}(\Psi_{dd}+1)}\,, \tag{6.12}$$

and the constants C_0 and C_1 are related to the background flow velocity, given by

$$C_0 = -(\hat{\lambda}_1 + 1)\left(\frac{Vx}{\tau_{\mathcal{G}}}\right) - 4\frac{V_x\Psi_{dd}}{\tau_{\mathcal{G}}}\,, \tag{6.13}$$

$$C_1 = -(\hat{\lambda}_0 + 1)\left(\frac{Vx}{\tau_{\mathcal{G}}}\right) + 4\frac{V_x\Psi_{dd}}{\tau_{\mathcal{G}}}\,. \tag{6.14}$$

The analytical solution for u_x and Ψ_{xd} is

$$u_x(t) = \frac{\mathcal{V}_0 + \mathcal{V}_1}{4\alpha}\,,\,, \tag{6.15}$$

$$\Psi_{xd}(t) = \frac{\left((\hat{\lambda}_0 + 1)\mathcal{V}_0 + (\hat{\lambda}_1 + 1)\mathcal{V}_1\right)}{8\alpha}\,, \tag{6.16}$$

where

$$\mathcal{V}_0 = \left(2\Psi_{xd}(0) - (\hat{\lambda}_1 + 1.0)u_x(0) + \frac{C_0\tau_{\mathcal{G}}}{\hat{\lambda}_0}\right)\exp\left(\frac{\hat{\lambda}_0 t}{\tau_{\mathcal{G}}}\right) - \frac{C_0\tau_{\mathcal{G}}}{\hat{\lambda}_0} \tag{6.17}$$

$$\mathcal{V}_1 = \left(-2\Psi_{xd}(0) + (\hat{\lambda}_0 + 1)u_x(0) + \frac{C_1\tau_{\mathcal{G}}}{\hat{\lambda}_1}\right)\exp\left(\frac{\hat{\lambda}_1 t}{\tau_{\mathcal{G}}}\right) - \frac{C_1\tau_{\mathcal{G}}}{\hat{\lambda}_1}\,. \tag{6.18}$$

The analytical solution for Eq. (4.21), Θ_{xx} can be solved through the equation for the determinant of the 1D variance-covariance matrix as

$$\frac{\mathrm{d}\Psi_{dd}\Theta_{xx} - \Psi_{xd}^2}{\mathrm{d}t} = -\frac{2}{\tau_{\mathcal{G}}}(\Psi_{dd}\Theta_{xx} - \Psi_{xd}^2)\,, \tag{6.19}$$

since Ψ_{dd} is time invariant and the solution for Ψ_{xd} was found previously in Eq. (6.16). In 1D, Θ_{yy} and Θ_{zz} are already decoupled laws of natural growth and can be solved analytically from the equations

$$\frac{\mathrm{d}\Theta_{yy}}{\mathrm{d}t} = -\frac{2}{\tau_{\mathcal{G}}}\Theta_{yy}\,, \tag{6.20}$$

$$\frac{\mathrm{d}\Theta_{zz}}{\mathrm{d}t} = -\frac{2}{\tau_{\mathcal{G}}}\Theta_{zz}\,. \tag{6.21}$$

The remaining analytical expressions for the homogeneous solution of the primitive variables Θ_{xx}, Θ_{yy} and Θ_{zz} are therefore

$$\Theta_{xx}(t) = \frac{1}{\Psi_{dd}}\left(\left(\Theta_{xx}(0)\Psi_{dd} - \Psi_{xd}(0)^2\right)\exp\left(-2\frac{t}{\tau_{\mathcal{G}}}\right) + \Psi_{xd}(t)^2\right)\,, \tag{6.22}$$

$$\Theta_{yy}(t) = \Theta_{yy}(0)\exp\left(-2\frac{t}{\tau_{\mathcal{G}}}\right)\,, \tag{6.23}$$

$$\Theta_{zz}(t) = \Theta_{zz}(0)\exp\left(-2\frac{t}{\tau_{\mathcal{G}}}\right)\,. \tag{6.24}$$

6.3 Numerical Results - Polydisperse flow

6.3.1 Homogeneous Problem

The first problem considered is a spacially homogeneous test case where particles have a range of sizes and initial velocities. This situation illustrates the effect of the drag on particles with different sizes. The particles in the domain start with an average velocity of $5.0\,\mathrm{m/s}$, with a variance Θ_{xx} of $1.0\,\mathrm{m^2/s^2}$, and zero covariance, Ψ_{xd}. The initial distribution of particle diameters uses the log-normal distribution function which is generated with $\mu = \ln(28 \times 10^{-6})$ and $\Psi_{dd} = 0.25$. The parameters of the Stokes drag law are chosen such that the relaxation time of particles with the median diameter, $d = 28\,\mu\mathrm{m}$ is $\tau = 1\,\mathrm{s}$. Considering that the relaxation times depends on the size of particles it results that smaller particles will relax more quickly compared to larger particles.

In the homogeneous problem, the evolution of the distribution function of particles at a point is investigated. In this problem, the solution is not affected by the hyperbolic flux since all the spatial derivatives are zero. The exact solution of the distribution function is shown on the left of Figures 6.1 and 6.2, while the evolution of the distribution function predicted by the model is shown on the right. The primitive variable solution through time is shown in Figures 6.3. As expected, the small particles are decelerated much more quickly than the big particles, creating some covariance, Ψ_{xd}, in the distribution function.

The bigger particles eventually relax faster than the exact solution. The variance in particles velocity needs to maintain the Gaussian shape of the distribution function. Therefore, the model is unable to represent perfectly the shape of the exact solution. The average particle velocity is, however, well captured through time.

6.3.2 Riemann Problem

The second scenario considered is a Riemann problem, which is spacially varying. The problem is tested with different intensity of the source term to study the effect of the drag on the model. The domain of interest is chosen to be $0\,\mathrm{m} < x < 20\,\mathrm{m}$. The

number density of particles between 0 m and 10 m is set to 100 particles cubic meter with an average velocity of 5.0 m/s. The number density for the rest of the domain is set to 10.0 particles per cubic meter with zero velocity. In the whole domain, the variance in particles velocity is chosen to be $1.0\,\mathrm{m}^2/\mathrm{s}^2$. The same particle size distribution as used in the previous problem is again used. This problem will be tested with no drag $\tau = \infty$s, with medium drag, $\tau = 1.0$ s, and with strong drag, $\tau = 0.1$ s.

In this section, a CFL of 0.5 is used with a grid of 4,000 cells. The solution is compared to a typical Eulerian model used in commercial software, the single-velocity model previously described in Eq. (3.15) and (3.16). In the first problem, with no drag, the exact solution in all the macroscopic properties is continuous.Solutions are shown in Figure 6.4. The polydisperse Gaussian model, being a hyperbolic system, tries to replicate the solution through a series of discontinuities, but a significant difference is visible. As for the single-velocity model, the model not allowing a range of velocity in any point, provides a poor solution. By adding drag to the problem, the predictive solution of the Polydisperse Gaussian model is improved, as illustrated in Figure 6.5. Again the single-velocity model is not able to represent the physics of the problem. The solution for the variance in x-velocity relaxes faster than the exact solution but follows the same trend. The covariance, Ψ_{xd}, becomes positive in the whole domain since the small particle slow down faster. As such, the big particles, as seen on the plot of the average log of the diameter travel further. Finally, for an even stronger drag, the predictive solution of the Polydisperse Gaussian model gets even better, as shown in Figure 6.6. The prediction for the number density of particles and the average velocity is much closer and follows the same trend as the exact solution. Again, the variance in x-velocity for the predictive solution relaxes faster compared to the exact solution. The other moment, such as the covariance between the velocity of particle and the average log of the diameter and the average log diameter are much closer to the exact solution.

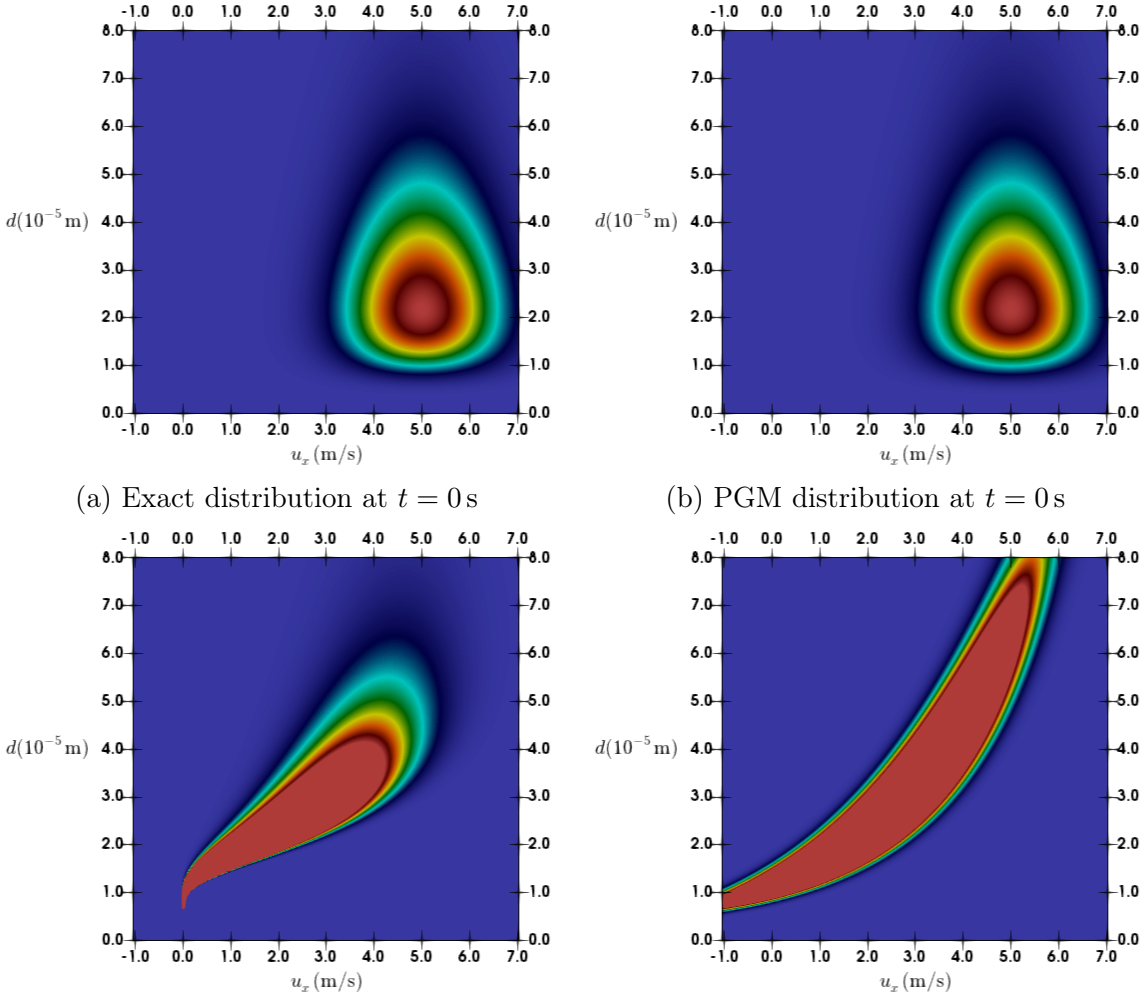

(a) Exact distribution at $t = 0\,\mathrm{s}$

(b) PGM distribution at $t = 0\,\mathrm{s}$

(c) Exact distribution at $t \approx 0.61\,\mathrm{s}$

(d) PGM distribution at $t \approx 0.61\,\mathrm{s}$

Figure 6.1: Slice plots in the $v_x - d$ plane showing the distribution function corresponding to a particle phase relaxing to a zero velocity background flow. The exact and PGM solutions are shown on the left and right sides, respectively, for the initial condition and time instance $t \approx 0.61\,\mathrm{s}$.

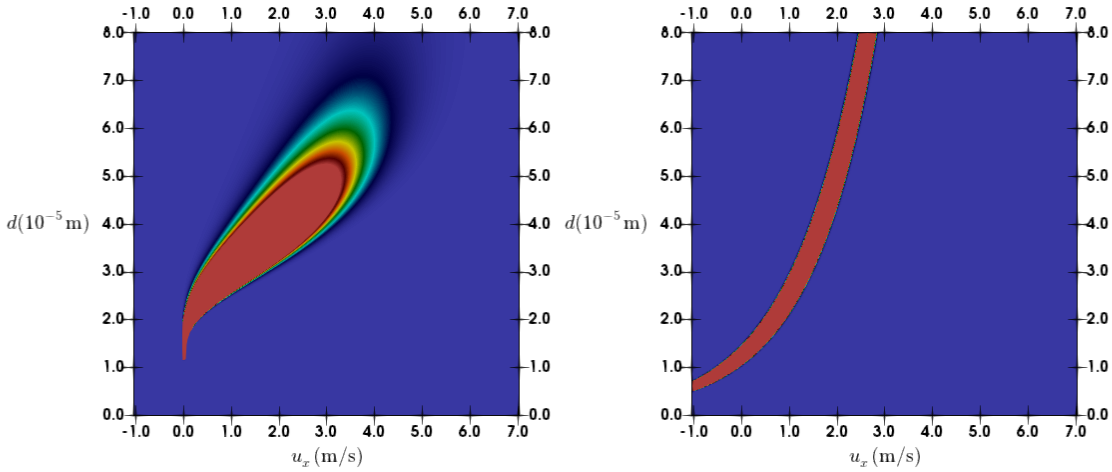

(a) Slice of the distribution function at $t \approx 1.82\,\mathrm{s}$

(b) Slice of the distribution function at $t \approx 1.82\,\mathrm{s}$

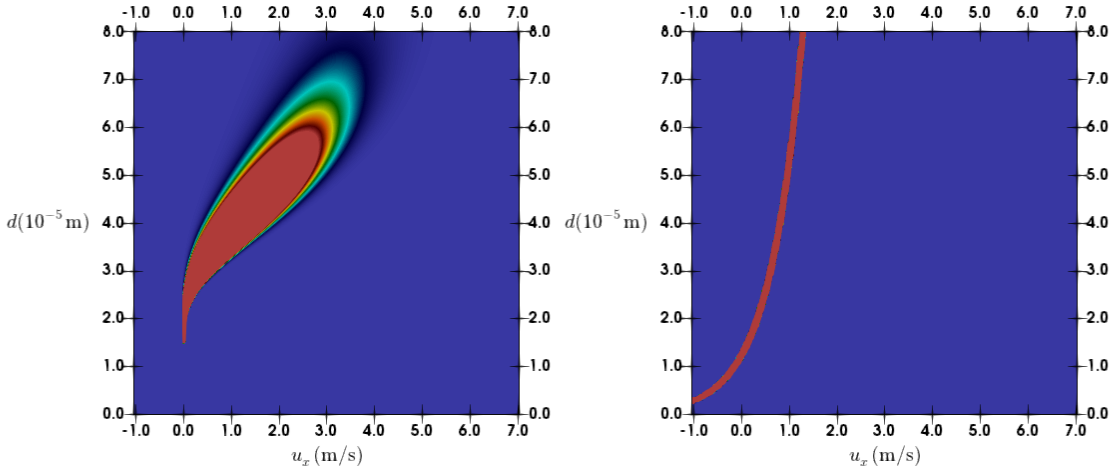

(c) Slice of the distribution function at $t \approx 3.03\,\mathrm{s}$

(d) Slice of the distribution function at $t \approx 3.03\,\mathrm{s}$

Figure 6.2: Slice plot in the $v_x - d$ plane showing the distribution function corresponding to a particle phase relaxing to a zero velocity background flow. The exact and PGM solutions are shown on the left and right sides, respectively, for time instances $t \approx 1.82\,\mathrm{s}$ and $t \approx 3.03\,\mathrm{s}$.

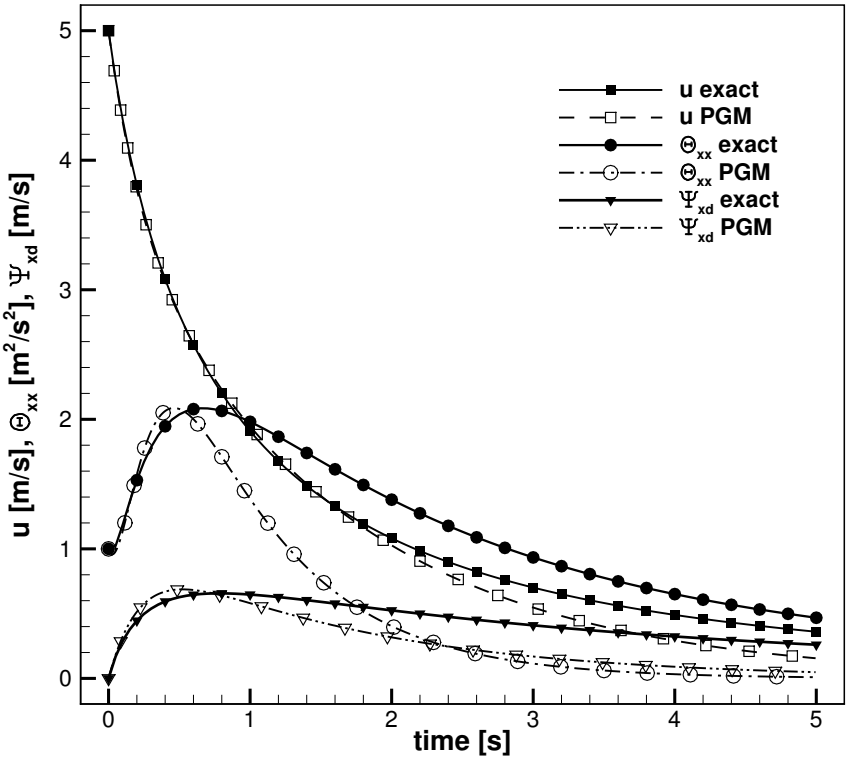

Figure 6.3: Exact and PGM evolution of the primitive variables for the space homogeneous problem described in the text.

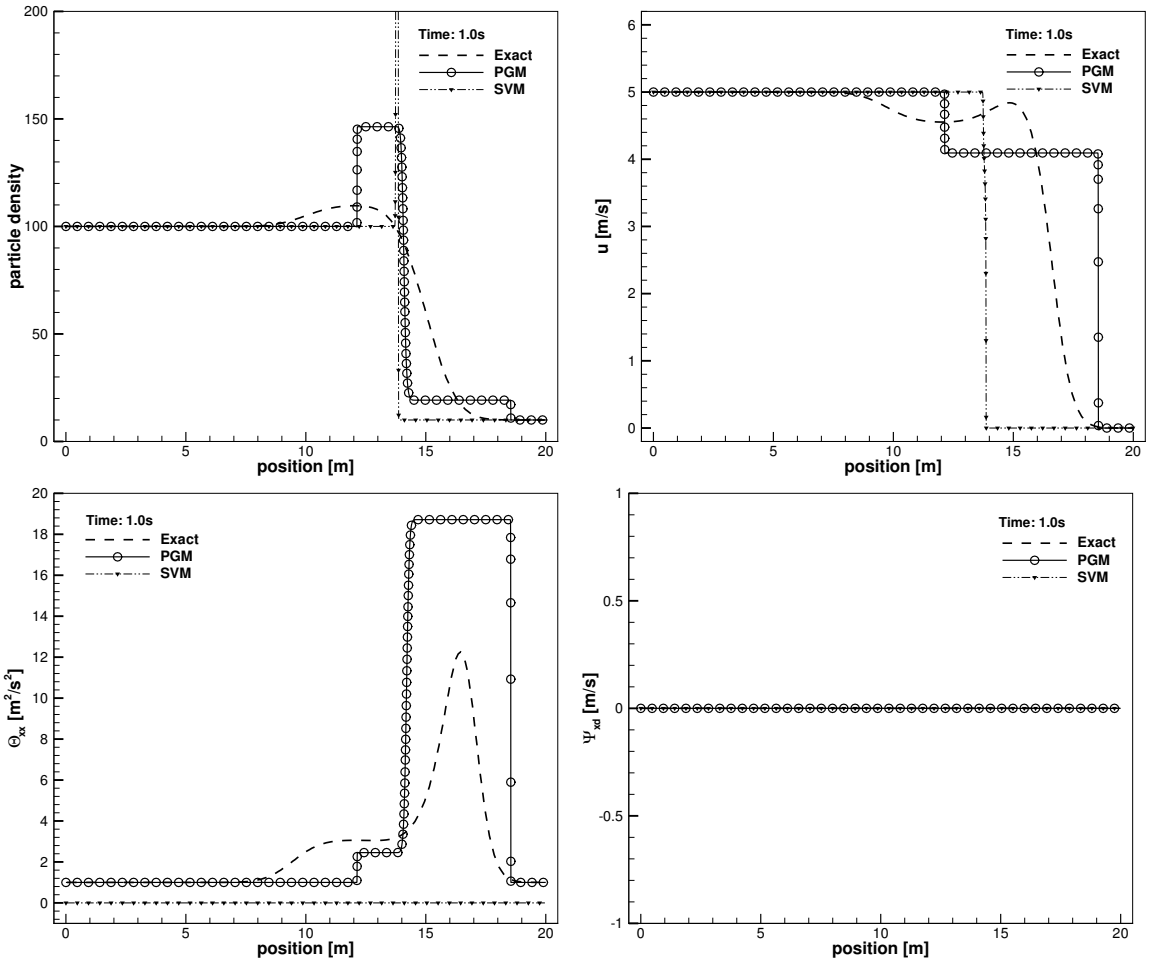

Figure 6.4: Predicted solution for various statistical properties for the Riemann problem test case described in the text. Results obtained in the case of no drag, $\tau = \infty$s, are depicted at $t = 1.0$ s.

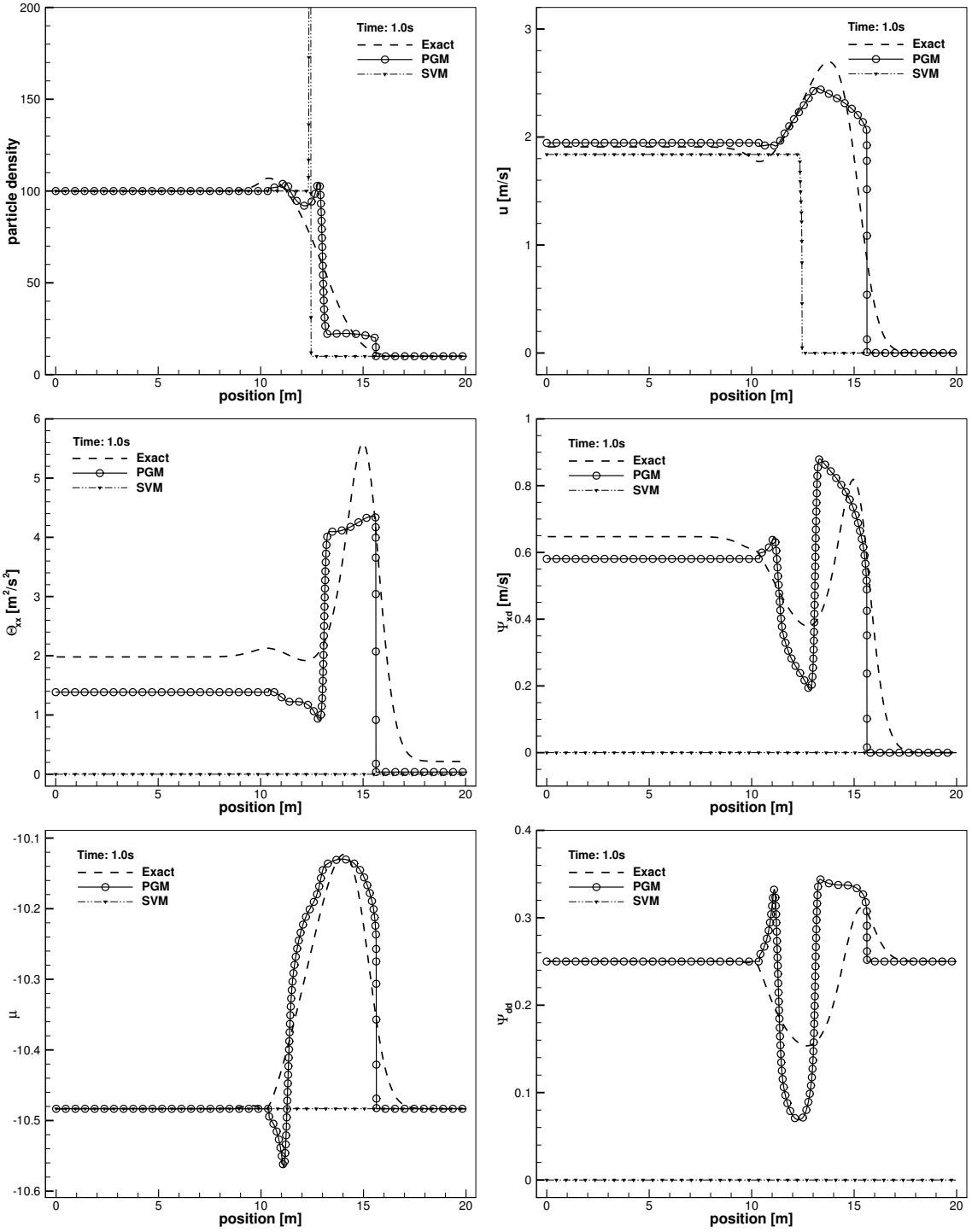

Figure 6.5: Predicted solution for various statistical properties for the Riemann problem test case described in the text. Results obtained for a medium drag relaxation time, $\tau = 1.0\,\mathrm{s}$, are depicted at $t = 1.0\,\mathrm{s}$.

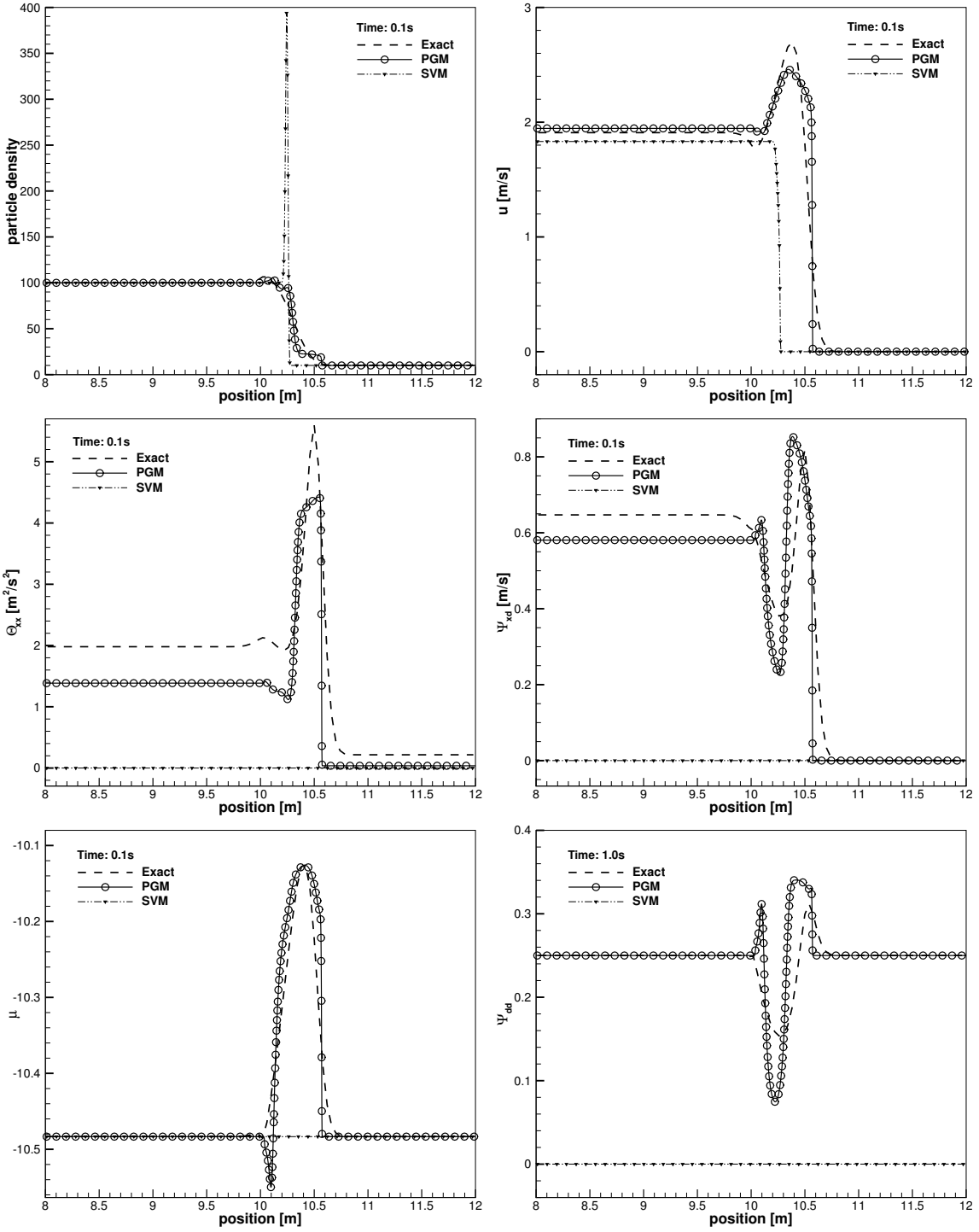

Figure 6.6: Predicted solution for various statistical properties for the Riemann problem test case described in the text. Results obtained for a strong drag relaxation time, $\tau = 0.1\,\mathrm{s}$, are depicted at $t = 0.1\,\mathrm{s}$.

Chapter 7

Conclusions and Future Work

7.1 Discussion and Conclusion

This research entailed the investigation of moment models for multiphase flow. It has been demonstrated that the higher-order moment-based models offer many advantages compared to traditional models. In particular, the ability of the fourteen-moment model to very accurately predict the repeated crossing of particle streams has been demonstrated. Additionally, it was demonstrated that lower-order members of the maximum-entropy hierarchy of models do not permit particle stream crossing. The example problem investigated here is, in one sense, a very difficult multiphase problem that contains repeated particle-trajectory crossings and multiple singularities in the solution. On the other hand, this problem has allowed the computation of the solution through the use of a one-dimensional algorithm. This simplification allowed a very high resolution to be used and very accurate numerical solutions to be obtained. Thus, the true predictive fidelity of the models themselves could be assessed. However, for a truly multi-dimensional situations, solutions will certainly be more computationally expensive and may be more difficult to obtain numerically for the higher-order moment models. The construction of a full-scale multi-dimensional flow solver using high-order moment models for multiphase flow prediction is the subject of continuing work. The high level of physical accuracy of the fourteen-moment model presented within this present work gives confidence that, if the PDEs can be solved accurately enough in higher dimensions, results will be equally good.

To predict particle dispersal resulting from an explosion of a radiological dispersal device, where particles have a range of particle sizes, the distribution function of the moment method needs to be extended into a diameter space. A new moment-based model for multiphase flows that is appropriate for such situations has been derived. An analysis of the new model has been shown and a proof of well-posedness has been

provided. A one-dimensional first-order Godunov finite-volume scheme has been implemented for the numerical solution of moment equations. Computations performed with this implementation demonstrates that the models can make predictions that are in good agreement with the underlying high-dimensional kinetic equation of such multiphase flow situations.

7.2 Future work

There are various potential avenues in which the current research can be extended. The new model is currently being investigated for more complex situations, including time-varying background flows that are typical of RDD explosions. The model will be extended to allow for a variety of drag laws that are applicable to a wider range of Stokes and Mach numbers.

The models is being extended and implemented within an existing higher-order accurate multi-dimensional numerical framework (2D and 3D). In this implementation, both the particle an carrier phases will be solved directly in a coupled manner. This will allow both the particle and gas phase to be simultaneously simulated.

References

[1] M. R. A. Abdelmalik and E. H. van Brummelen. An entropy stable discontinuous galerkin finite-element moment method for the boltzmann equation. *Computers & Mathematics with Applications*, 72(8):1988–1999, 2016.

[2] T. J. Barth. On discontinuous Galerkin approximations of boltzmann moment systems with Levermore closure. *Computer Methods in Applied Mechanics and Engineering*, 195:3311–3330, 2006.

[3] Bragg, D. C. Swailes, and R. Skartlien. Drift-free kinetic equations for turbulent dispersion. *Physica A*, 86(056306), 2012.

[4] F. Brini. Hyperbolicity region in extended thermodynamics with 14 moments. *Continuum Mechanics and Thermodynamics*, 13:1–8, 2001.

[5] S. L. Brown. *Approximate Riemann Solvers for Moment Models of Dilute Gases*. PhD thesis, University of Michigan, 1996.

[6] S. L. Brown, P. L. Roe, and C. P. T. Groth. Numerical solution of a 10-moment model for nonequilibrium gasdynamics. Paper 95-1677, AIAA, June 1995.

[7] Z. Ben Dia. Novel treatments for multi-pahse flow prediction inspired by kinetic theory. Master's thesis, University of Ottawa, 2016.

[8] W. Dreyer. Maximization of the entropy in non-equilibrium. *Journal of Physics A: Mathematical and General*, 20:6505–6517, 1987.

[9] François Forgues and James G. McDonald. Higher-order moment models for laminar multiphase flows with accurate particle-stream crossing. *International Journal of Multiphase Flow*, 114:28 – 38, 2019.

[10] R. O. Fox. A quadrature based third-order moment method for dilute gas-particle flows. *Journal of Computational Physics*, 227:6313–6350, 2008.

[11] R. O. Fox. Higher-order quadrature-based moment methods for kinetic equations. *Journal of Computational Physics*, 228:7771–7791, 2009.

[12] K. O. Friedrichs and P. D. Lax. Systems of conservation laws with a convex extension. *ProcNAS*, 68:1686–1688, 1971.

[13] S. K. Godunov. Finite-difference method for numerical computations of discontinuous solutions of the equations of fluid dynamics. *Matematicheskii Sbornik*, 47:271–306, 1959.

[14] S. K. Godunov. An interesting class of quasilinear systems. *Soviet Mathematics Doklady*, 2:947–949, 1961.

[15] T. I. Gombosi. *Gaskinetic Theory*. Cambridge University Press, Cambridge, 1994.

[16] H. Grad. On the kinetic theory of rarefied gases. *Communications on Pure and Applied Mathematics*, 2:331–407, 1949.

[17] A. Haider and O. Levenspiel. Drag coefficient and terminal velocity of spherical and nonspherical particles. *Powder Technology*, 58:63–70, 1989.

[18] A. Harten, P. D. Lax, and B. van Leer. On upstream differencing and Godunov-type schemes for hyperbolic conservation laws. *SIAM Review*, 25(1):35–61, 1983.

[19] C. D. Hauck, C. D. Levermore, and A. L. Tits. Convex duality and entropy-based moment closures: Characterizing degenerate densities. *SIAM Journal on Control and Optimization*, 47(4):1977–2015, 2008.

[20] L. Ivan, D. Hummel, and L. Lebel. Hyperbolic conservation laws on three-dimensional a mcrexs modelling approach for the simulation of radiological dispersal device. *Journal of Environmental Radioactivity*, 192:551–564, 2018.

[21] M. Junk. Domain of definition of Levermore's five-moment system. *Journal of Statistical Physics*, 93(5/6):1143–1167, 1998.

[22] M. Junk and A. Unterreiter. Maximum entropy moment systems and Galilean invariance. *Continuum Mechanics and Thermodynamics*, 14:563–576, 2002.

[23] G. M. Kremer. *An Introduction to the Boltzmann Equation and Transport Processes in Gases*. Springer-Verlag, Berlin, 2010.

[24] L. D. Landau and E. M. Lifshitz. *Fluid Mechanics*. Pergamon Press, Oxford, England, 2nd edition, 1987.

[25] C. D. Levermore. Moment closure hierarchies for kinetic theories. *Journal of Statistical Physics*, 83:1021–1065, 1996.

[26] C. D. Levermore and W. J. Morokoff. The Gaussian moment closure for gas dynamics. *SIAM Journal on Applied Mathematics*, 59(1):72–96, 1998.

[27] Daniele L. Marchisio and Rodney O. Fox. *Computational Models for Polydisperse Particulate and Multiphase Systems*. Cambridge Series in Chemical Engineering. Cambridge University Press, 2013.

[28] M. R. Maxey and J. J. Riley. Equation of motion for a small rigid sphere in a uniform flow. *Physics of Fluids*, 26(4):883–889, 1983.

[29] J. G. McDonald. *Extended Fluid-Dynamic Modelling for Numerical Solution of Micro-Scale*. PhD thesis, University of Toronto, 2011.

[30] J. G. McDonald, J. S. Sachdev, and C. P. T. Groth. Application of Gaussian moment closure to micro-scale flows with moving and embedded boundaries. *AIAA Journal*, 52:1839–1857, 2014.

[31] J. G. McDonald and M. Torrilhon. Affordable robust moment closures for CFD based on the maximum-entropy hierarchy. *Journal of Computational Physics*, 251:500–523, 2013.

[32] James G. McDonald. Approximate maximum-entropy moment closures for gas dynamics. *AIP Conference Proceedings*, 1786(1):140001, 2016.

[33] E.E. Michaelides, C. T. Crowe, and J. Schwarzkopf, editors. *Multiphase Flow Handbook*, chapter Computational Methods, pages 144 – 202. CRC Press, 2nd edition edition, 2017.

[34] I. Müller. *Thermodynamics*. Pitman Publishing, Boston, 1985.

[35] I. Müller and T. Ruggeri. *Rational Extended Thermodynamics*. Springer-Verlag, New York, 1998.

[36] M. W. Reeks. On a kinetic equation for the transport of particle in turbulent flows. *Physics of Fluids A*, 3(3):446 – 456, 1991.

[37] M. W. Reeks. On the continuum equations for dispersed particles in non uniform flow. *Physics of Fluids A*, 4(6):1290 – 1303, 1992.

[38] P. L. Roe. Characteristic-based schemes for the Euler equations. *Annual Review of Fluid Mechanics*, 18:337–365, 1986.

[39] G. Rudinger. *Fundamentals of Gas-Particle Flow*. Elsevier Scientific Publishing Company, Amsterdam, 1980.

[40] R. Saurel, E. Daniel, and J. C. Loraud. Two-phase flows: Second-order schemes and boundary conditions. *AIAA Journal*, 32(6):1214–1221, June 1994.

[41] L. Schiller and A. Naumann. A drag coefficient correlation. *V.D.I. Zeitung*, 77:318–320, 1935.

[42] S. A. Slater and J. B. Young. The calculation of inertial particle transport in dilute gas-particle flows. *International Journal of Multiphase Flow*, 27:61–87, 2001.

[43] H. Struchtrup. *Macroscopic Transport Equations for Rarefied Gas Flows*. Springer-Verlag, Berlin, 2005.

[44] H. Struchtrup and M. Torrilhon. Regularization of Grad's 13 moment equations: Derivation and linear analysis. *Physics of Fluids*, 15(9):2668–2680, 2003.

[45] Y. Suzuki and B. van Leer. Application of the 10-moment model to MEMS flows. Paper 2005-1398, AIAA, January 2005.

[46] D. C. Swailes and K. F. F. Darbyshire. A generalised fokker-planck equation for particle transport in random media. *Physica A*, 242:38–48, 1997.

[47] B. R. Tensuda, J. G. McDonald, and C. P. T. Groth. Application of a maximum-entropy-based 14-moment closure for multi-dimensional non-equilibrium flows. Paper 2015-3420, AIAA, June 2015.

[48] M. Torrilhon. Characteristic waves and dissipation in the 13-moment-case. *Continuum Mechanics and Thermodynamics*, 12:289–301, 2000.

[49] M. Torrilhon. Hyperbolic moment equations in kinetic gas theory based on multivariate Pearson-IV-distributions. *Communications in Computational Physics*, 7(4):639–673, 2010.

[50] R. Turton and O. Levenspiel. A short note on the drag correlation for spheres. *Powder Technology*, 47:83–86, 1986.

[51] A. Vié, F. Doisneau, and M. Massot. On the anisotropic Gaussian velocity closure for inertial-particle laden flows. *Communications in Computational Physics*, 17(1):1–46, 2015.

[52] F. A. Williams. Spray Combustion and Atomization. *Physics of Fluids*, 1:541–545, November 1958.

[53] C. Yuan and R. O. Fox. Conditional quadrature method of moments for kinetic equations. *Journal of Computational Physics*, 2011.

[54] L. I. Zaichik, V. M. Aliphenkov, and E. G. Sinaiski. *Particles in Turbulent Flows*. Willey-VCH, 2008.

Appendix A

Exact Solution for Particle flow with Stokes Drag and Zero Background Velocity

Starting from the Boltzmann equation with no collision

$$\frac{\partial \mathcal{F}}{\partial t} + v_\alpha \frac{\partial \mathcal{F}}{\partial x_\alpha} + \frac{\partial}{\partial v_\alpha}\left(a_\alpha \mathcal{F}\right) = 0\,, \tag{A.1}$$

where $\mathcal{F}$ is a function of $\mathcal{F}(x_i, v_i, d, t)$ and the acceleration term is

$$a_i = \frac{V_i - v_i}{\tau} \quad \text{with} \qquad \tau = \frac{\phi}{d^2} \quad \text{and} \qquad \phi = \frac{18\mu_f}{\rho_p}$$

The domain is taken to be $-\infty < \mathrm{x} < \infty$ and $-\infty < \mathrm{v_i} < \infty$ and the initial distribution function is taken as

$$\mathcal{F}(x_i, v_i, d, 0) = \mathcal{F}_0(x_i, v_i, d)\,. \tag{A.2}$$

Assuming that the distribution is a function of

$$\mathcal{F}(x_i, v_i, d, t) = A(t)\ \mathcal{F}_0(B_j(x_i, v_i, d, t), C_j(v_j, d, t), d)\,.$$

The time, space and velocity partial derivative of the distribution function can be written as

$$\frac{\partial \mathcal{F}}{\partial t} = \mathcal{F}_0 \frac{\partial A}{\partial t} + A\frac{\partial \mathcal{F}_0}{\partial t} = \mathcal{F}_0 \frac{\partial A}{\partial t} + A\frac{\partial \mathcal{F}_0}{\partial B_j}\frac{\partial B_j}{\partial t} + A\frac{\partial \mathcal{F}_0}{\partial C_j}\frac{\partial C_j}{\partial t}\,,$$

$$\frac{\partial \mathcal{F}}{\partial x_i} = A\frac{\partial \mathcal{F}_0}{\partial B_j}\frac{\partial B_j}{\partial x_i}\,,$$

$$\frac{\partial}{\partial v_i}\left(\frac{\phi}{d^2} v_i \mathcal{F}\right) = \frac{\phi}{d^2}\left(\frac{\partial v_i}{\partial vi}\mathcal{F} + v_i \frac{\partial \mathcal{F}}{\partial v_i}\right) = \frac{\phi}{d^2} 3\mathcal{F} + \frac{\phi v_i}{d^2}\left(\frac{\partial \mathcal{F}_0}{\partial B_j}\frac{\partial B_j}{\partial v_i} + \frac{\partial \mathcal{F}_0}{\partial C_j}\frac{\partial C_j}{\partial v_i}\right)\,.$$

Adding these back to the boltzmann equation the evolution of the distribution function can now be expressed as

$$\mathcal{F}_0\frac{\partial A}{\partial t} + A\frac{\partial \mathcal{F}_0}{\partial B_j}\frac{\partial B_j}{\partial t} + A\frac{\partial \mathcal{F}_0}{\partial C_j}\frac{\partial C_j}{\partial t} + v_i A\frac{\partial \mathcal{F}_0}{\partial B_j}\frac{\partial B_j}{\partial x_i} - 3\frac{\phi}{d^2}\mathcal{F} - A\frac{\phi v_i}{d^2}\left(\frac{\partial \mathcal{F}_0}{\partial B_j}\frac{\partial B_j}{\partial v_i} + \frac{\partial \mathcal{F}_0}{\partial C_j}\frac{\partial C_j}{\partial v_i}\right) = 0$$

This expands to

$$\overbrace{\mathcal{F}_0\frac{\partial A}{\partial t}-3\frac{\phi A}{d^2}\mathcal{F}_0}^{(3)}+\frac{\partial \mathcal{F}_0}{\partial B_j}\overbrace{\left(A\frac{\partial B_j}{\partial t}+Av_i\frac{\partial B_j}{\partial x_i}+\frac{\phi}{d^2}Av_i\frac{\partial B_j}{\partial v_i}\right)}^{(2)}+\frac{\partial \mathcal{F}_0}{\partial C_j}\overbrace{\left(A\frac{\partial C_j}{\partial t}-\frac{\phi A v_i}{d^2}\frac{\partial C_j}{\partial v_i}\right)}^{(1)}=0$$

For this equation to be true, each part must be zero independently. If we take part 1,

$$\frac{\partial C_j}{\partial t}-\frac{\phi A v_i}{d^2}\frac{\partial C_j}{\partial v_i}=0\,.$$

For this relation to be satisfied C_j must be equal to $v_j e^{\frac{\phi t}{d^2}}$. In part 2 of the equation,

$$\frac{\partial B_j}{\partial t}+v_i\frac{\partial B_j}{\partial x_i}+\frac{\phi}{d^2}v_i\frac{\partial B_j}{\partial v_i}=0\,,$$

B_j must be equal to $x_j+v_j\frac{d^2}{\phi}(1-e^{\frac{\phi t}{d^2}})$. Finally, for part 3,

$$\mathcal{F}_0\frac{\partial A}{\partial t}-3\frac{\phi A}{d^2}\mathcal{F}_0=0\,,$$

A is found to be $e^{\frac{3\phi t}{d^2}}$. The exact solution at any future time is now given by

$$\mathcal{F}(x_i,v_i,d,t)=A\,\mathcal{F}_0(B_i,C_i,d)\,. \tag{A.3}$$